

## RESEARCH ARTICLE

10.1002/2015GB005300

## Special Section:

Trends and Determinants of the Amazon Rainforests in a Changing World, A Carbon Cycle Perspective

## Key Points:

- Amazon Basin emits 31–42 Tg (methane)/yr in 2010–2011
- Basin contributes significantly (up to 7.5%) to global methane emissions
- Total noncombustion basin emissions were similar in 2010 and 2011

## Supporting Information:

- Figure S1 and Table S1

## Correspondence to:

C. Wilson,  
c.wilson@leeds.ac.uk

## Citation:

Wilson, C., M. Gloor, L. V. Gatti, J. B. Miller, S. A. Monks, J. McNorton, A. A. Bloom, L. S. Basso, and M. P. Chipperfield (2016), Contribution of regional sources to atmospheric methane over the Amazon Basin in 2010 and 2011, *Global Biogeochem. Cycles*, 30, doi:10.1002/2015GB005300.

Received 5 OCT 2015

Accepted 3 FEB 2016

Accepted article online 6 FEB 2016

©2016. The Authors.

This is an open access article under the terms of the Creative Commons Attribution License, which permits use, distribution and reproduction in any medium, provided the original work is properly cited.

## Contribution of regional sources to atmospheric methane over the Amazon Basin in 2010 and 2011

Chris Wilson<sup>1,2,3</sup>, Manuel Gloor<sup>3</sup>, Luciana V. Gatti<sup>4</sup>, John B. Miller<sup>5,6</sup>, Sarah A. Monks<sup>2,7,8</sup>, Joey McNorton<sup>1,2</sup>, A. Anthony Bloom<sup>9</sup>, Luana S. Basso<sup>4</sup>, and Martyn P. Chipperfield<sup>1,2</sup>

<sup>1</sup>National Centre for Earth Observation, University of Leeds, Leeds, UK, <sup>2</sup>School of Earth and Environment, University of Leeds, Leeds, UK, <sup>3</sup>School of Geography, University of Leeds, Leeds, UK, <sup>4</sup>Instituto de Pesquisas Energéticas e Nucleares, Comissão Nacional de Energia Nuclear, Atmospheric Chemistry Laboratory, Sao Paulo, Brazil, <sup>5</sup>Global Monitoring Division, Earth System Research Laboratory, National Oceanic and Atmospheric Administration, Boulder, Colorado, USA, <sup>6</sup>Cooperative Institute for Research in Environmental Sciences, University of Colorado Boulder, Boulder, Colorado, USA, <sup>7</sup>Now at Chemical Sciences Division, Earth System Research Laboratory, National Oceanic and Atmospheric Administration, Boulder, Colorado, USA, <sup>8</sup>Now at Cooperative Institute for Research in Environmental Sciences, University of Colorado Boulder, Boulder, Colorado, USA, <sup>9</sup>Jet Propulsion Laboratory, California Institute of Technology, Pasadena, California, USA

**Abstract** We present an assessment of methane (CH<sub>4</sub>) atmospheric concentrations over the Amazon Basin for 2010 and 2011 using a 3-D atmospheric chemical transport model, two wetland emission models, and new observations made during biweekly flights made over four locations within the basin. We attempt to constrain basin-wide CH<sub>4</sub> emissions using the observations, and since 2010 was an unusually dry year, we assess the effect of this drought on Amazonian methane emissions. We find that South American emissions contribute up to 150 ppb to concentrations at the sites, mainly originating from within the basin. Our atmospheric model simulations agree reasonably well with measurements at three of the locations ( $0.28 \leq r^2 \leq 0.63$ , mean bias  $\leq 9.5$  ppb). Attempts to improve the simulated background CH<sub>4</sub> concentration through analysis of simulated and observed sulphur hexafluoride concentrations do not improve the model performance, however. Through minimisation of seasonal biases between the simulated and observed atmospheric concentrations, we scale our prior emission inventories to derive total basin-wide methane emissions of 36.5–41.1 Tg(CH<sub>4</sub>)/yr in 2010 and 31.6–38.8 Tg(CH<sub>4</sub>)/yr in 2011. These totals suggest that the Amazon contributes significantly (up to 7%) to global CH<sub>4</sub> emissions. Our analysis indicates that factors other than precipitation, such as temperature variations or tree mortality, may have affected microbial emission rates. However, given the uncertainty of our emission estimates, we cannot say definitively whether the noncombustion emissions from the region were different in 2010 and 2011, despite contrasting meteorological conditions between the two years.

### 1. Introduction

Methane (CH<sub>4</sub>) is a powerful greenhouse gas that is emitted into the atmosphere from a variety of anthropogenic and natural sources. As the second most important long-lived atmospheric greenhouse gas [Myhre *et al.*, 2013], it has an influential role on the Earth's climate and on the oxidizing capacity of the troposphere [Prather *et al.*, 2001]. Natural wetlands, the largest single source of methane into the atmosphere (110–284 Tg (CH<sub>4</sub>)/yr) [Matthews and Fung, 1987; Kirschke *et al.*, 2013], make up around 20–40% of the total natural and anthropogenic sources of atmospheric methane. Due to the sensitivity of wetland emissions to climate factors such as temperature and precipitation, these emissions may significantly affect the interannual variation of atmospheric CH<sub>4</sub> [Fung *et al.*, 1991; Bousquet *et al.*, 2006; Kirschke *et al.*, 2013; Pison *et al.*, 2013]. Similarly, CH<sub>4</sub> emissions from biomass burning exhibit large interannual variability due to the dependence of fire occurrence and intensity on meteorological conditions [van der Werf *et al.*, 2010]. Due partly to the variable contribution of these natural sources, along with variations in climate [Rigby *et al.*, 2008] and the relatively short lifetime of CH<sub>4</sub> (9–11 years) [Prinn *et al.*, 2005; Fiore *et al.*, 2008; Prather *et al.*, 2012], the annual growth rate of atmospheric methane varies significantly over short time scales (e.g., a few years). After a period of growth throughout the 1990s, the atmospheric growth rate of CH<sub>4</sub> averaged approximately zero for the period 2000–2006, after which it once again rose steadily until the present [Dlugokencky *et al.*, 2011; Nisbet *et al.*, 2014]. Total methane emissions, as well as the partitioning of emissions between different source types, are not well constrained, and although several hypotheses have been proposed to explain the recent

stabilization and subsequent regrowth of the atmospheric CH<sub>4</sub> budget, none of them has yet been proven conclusively. Proposed explanations of the recent stalling have included a decrease in emissions from fossil fuels [e.g., *Aydin et al.*, 2011; *Simpson et al.*, 2012; *Kirschke et al.*, 2013], stabilization of both fossil fuel and microbial sources [*Levin et al.*, 2012], reductions in emissions from rice paddies due to improvements in practices [*Kai et al.*, 2011], and variations in the magnitude of the atmospheric sink of CH<sub>4</sub> [*Rigby et al.*, 2008; *Montzka et al.*, 2011]. However, without better evaluation of CH<sub>4</sub> surface fluxes, particularly from tropical regions, it is difficult to properly attribute changes in the atmospheric growth rate to variations in sources and sinks.

The total global emission of methane into the atmosphere from wetland sources depends both on global wetland extent and on methane emission rate, although neither of these factors is currently well constrained [*Ringeval et al.*, 2010; *Melton et al.*, 2013]. The tropical regions make up the majority (50–60%) of the total global natural wetland CH<sub>4</sub> source [e.g., *Cao et al.*, 1996; *Bloom et al.*, 2010, 2012], and inundated wetland regions in the Amazon Basin of South America, which covers an area of approximately 6,000,000 km<sup>2</sup> [*Poulter et al.*, 2010], have been estimated to contribute significantly (24%) [*Bloom et al.*, 2012]. Previous estimates of CH<sub>4</sub> emissions from the basin range from 4 to 92 Tg(CH<sub>4</sub>)/yr [*do Carmo et al.*, 2006; *Kirschke et al.*, 2013], but until recently, a scarcity of in situ observations of atmospheric CH<sub>4</sub> concentrations in this region has restricted the possibility of thorough evaluation of these emission estimates.

There have been previous attempts to use inverse modeling methods along with satellite observations of atmospheric CH<sub>4</sub> concentrations in order to constrain emissions from the basin. However, due to limitations such as retrieval errors, the limited accuracy and coverage of remotely sensed CH<sub>4</sub> over the region, and a lack of in situ measurements, these studies obtained artificially large total emissions [*Frankenberg et al.*, 2006, 2008] or relatively small uncertainty reductions compared to better-observed regions [e.g., *Bergamaschi et al.*, 2009; *Fraser et al.*, 2013].

In 2010, to remedy this situation, we initiated regular measurements of various atmospheric species, including CH<sub>4</sub>, carbon monoxide (CO), carbon dioxide (CO<sub>2</sub>), and sulphur hexafluoride (SF<sub>6</sub>), at four sites within the Amazon Basin [*Gatti et al.*, 2014]. On an approximately biweekly basis, vertical profiles of these species are measured over four locations at Santarem (SAN), Rio Branco (RBA), Tabatinga (TAB), and Alta Floresta (ALF), all of which are in the Brazilian part of the Amazon Basin (see Figure 1). These vertical profiles extend from just above the forest canopy to approximately 4.4 km above sea level, and the locations were selected to be sensitive to fluxes from the entire basin.

This study uses these new observations of CH<sub>4</sub>, CO, and SF<sub>6</sub> along with a chemical transport model, TOMCAT [*Chipperfield*, 2006], and two wetland emission models [*Clark et al.*, 2011; *Bloom et al.*, 2012] to reduce the uncertainty regarding methane emissions from the Amazon Basin during 2010 and 2011 and to assess the interannual uncertainty. We link differences between observed and simulated SF<sub>6</sub> concentrations at the Amazonian measurement sites to errors in the model latitudinal transport. Quantifying this model transport error then allows us to update the simulated background CH<sub>4</sub> concentrations at each of the sites. The use of tagged tracers in the transport model simulations also allows us to attribute variations in CH<sub>4</sub> in the lower troposphere to different source types. Fortunately, our chosen time period allows us also to assess to some extent the effect of drought on CH<sub>4</sub> emissions in the region, since the Amazon suffered extremely dry conditions in 2010, while 2011 was an unusually wet year [*Lewis et al.*, 2011; *Gatti et al.*, 2014]. Figure 2 shows the variations in precipitation and temperature in the region for the two years in question, highlighting the unusual conditions affecting the basin in 2010 in particular. Previous studies have attempted to evaluate simulations of CH<sub>4</sub> using in situ observations made far downwind of the basin or with remote sensing observations of CH<sub>4</sub> from satellites [e.g., *Frankenberg et al.*, 2008; *Bergamaschi et al.*, 2009; *Fraser et al.*, 2013]. These studies were therefore unable to directly assess local emissions of CH<sub>4</sub>, a problem that the observations made for this study allow us to overcome.

The rest of this study is structured as follows. Section 2 describes the new measurements of atmospheric CH<sub>4</sub>, CO, and SF<sub>6</sub> concentrations above the basin. Section 3 outlines our methodology and describes the version of the TOMCAT model and the emission inventories that were used. Section 4 describes the findings derived from the observations and model simulations and discusses their implications for constraining CH<sub>4</sub> emissions from the basin. Finally, we summarize the results in section 5.

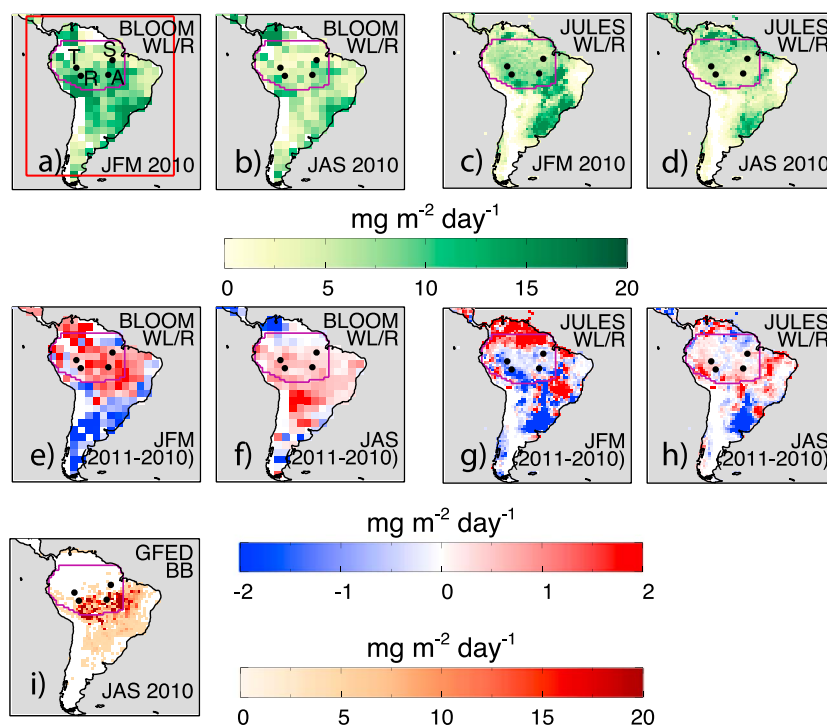


**Figure 1.** Wetland and rice paddy (WL/R)  $\text{CH}_4$  ( $\text{mg CH}_4 \text{ m}^{-2} \text{ d}^{-1}$ ) South American emission estimates used in this study for JFM and JAS 2010 using (Figures 1a and 1b) the method of *Bloom et al.* [2012] and (Figures 1c and 1d) JULES land surface model. Change in WL/R emissions ( $\text{mg CH}_4 \text{ m}^{-2} \text{ d}^{-1}$ ) between 2011 and 2010 in JFM and JAS using (e and f) the method of *Bloom et al.* [2012] and (g and h) JULES model. (i) Biomass burning (BB) emissions ( $\text{mg CH}_4 \text{ m}^{-2} \text{ d}^{-1}$ ) [*van der Werf et al.*, 2010] in JAS 2010. Emissions from biomass burning and JULES model are shown on  $1^\circ \times 1^\circ$  resolution, while BLOOM emissions have horizontal resolution of  $3^\circ \times 3^\circ$ . The region defined as the Amazon Basin in this study is indicated by the purple boundary. Figure 1a also shows the region defined in the model as South America, indicated by the red box, outside of which modeled  $\text{CH}_4$  is partitioned into the background tracer. Both regions are defined in the text. The location of the observation sites Santarem (S), Tabatinga (T), Alta Floresta (A), and Rio Branco (R) are also indicated in Figure 1a.

## 2. Observations

Since 2010, aircraft-borne flask air observations of a number of species, including  $\text{CH}_4$ ,  $\text{CO}$ , and  $\text{SF}_6$ , have been made at four Amazon sites (shown in Figure 1) by researchers at the Instituto de Pesquisas Energéticas e Nucleares (IPEN) in Sao Paulo, Brazil, in collaboration with the University of Leeds, UK, and the Earth System Research Laboratory of the National Oceanic and Atmospheric Administration (NOAA/ESRL) in Boulder, CO, USA. The sites are located at Santarem (SAN,  $55.0^\circ\text{W}$ ,  $2.9^\circ\text{S}$ ), Tabatinga (TAB,  $69.7^\circ\text{W}$ ,  $6.0^\circ\text{S}$ ), Alta Floresta (ALF,  $56.7^\circ\text{W}$ ,  $8.9^\circ\text{S}$ ), and Rio Branco (RBA,  $67.9^\circ\text{W}$ ,  $9.3^\circ\text{S}$ ). Figure 1a shows the location of these measurement sites within the basin. Flights are undertaken at approximately biweekly intervals above each site up to an altitude of  $\sim 4.4$  km, and 0.7 L flasks were filled every 300–500 m in order to provide vertical profiles. All measurements were taken between 12:00 and 13:00 local time, when the boundary layer is close to being fully developed. Flask air was subsequently analyzed for  $\text{CH}_4$ ,  $\text{CO}_2$ ,  $\text{CO}$ ,  $\text{N}_2\text{O}$ , and  $\text{SF}_6$  concentrations at the high-precision gas analytics laboratory of L. Gatti at IPEN. For more information about these measurements, see *Gatti et al.* [2014]. The measurement locations were chosen in order to sample the dominant tropospheric airstream across the basin, in which air enters from the northeast and sweeps toward the mountainous regions to the west of the basin before turning back toward the southeast of the basin and the Atlantic Ocean [*Gatti et al.*, 2014]. Thus, the two western sites (RBA and TAB) sample air that is representative of a large proportion of the tropical rainforest within the basin. Observations made at the eastern sites (SAN and ALF) sample air that is influenced by a smaller proportion of the basin, representative not only of forests but also of contributions from savannah and agricultural land.

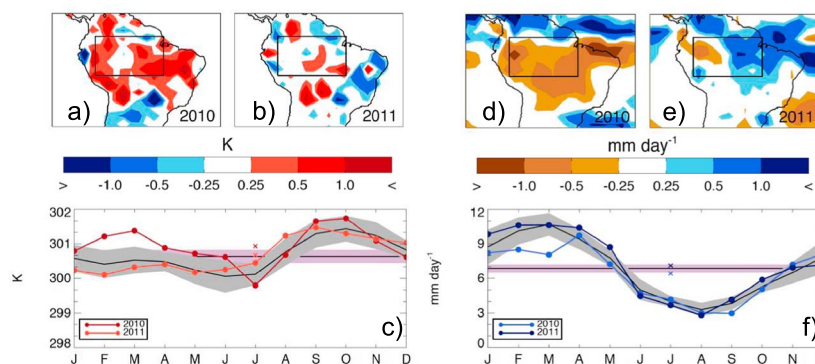


**Figure 2.** Temperature anomaly (K) in (a) 2010 and (b) 2011 calculated as the annual mean differences from the average for 2004–2011. Data taken from the Global Historical Climatology Network version 2 and the Climate Anomaly Monitoring System ( $0.5^\circ \times 0.5^\circ$ ) (accessed from [www.esrl.noaa.gov/psd/](http://www.esrl.noaa.gov/psd/)) [Fan and van den Dool, 2008]. (c) Monthly mean Amazon Basin temperature (K) for 2010 (dark red) and 2011 (light red). Thick black line with gray shaded area shows climatology and  $1\sigma$  deviation over the period 2004–2011. Crosses represent annual mean temperature for the two years, and thin black line with purple shaded area represents mean annual temperature for 2004–2011 and  $1\sigma$  deviation. Precipitation anomaly (mm/d) in (d) 2010 and (e) 2011 calculated as the annual mean difference from the average for 2004–2011. Data taken from the Global Precipitation Climatology Project ( $2.5^\circ \times 2.5^\circ$ ) for the Southern Hemisphere Amazon Basin (accessed from [www.esrl.noaa.gov/psd/](http://www.esrl.noaa.gov/psd/)) [Beck et al., 2005]. (f) Monthly mean Amazon Basin precipitation (mm/d) for 2010 (light blue) and 2011 (dark blue).

### 3. Model Setup

TOMCAT is a Eulerian, offline three-dimensional (3-D) chemical transport model (CTM), described in Chipperfield et al. [1993]; Stockwell and Chipperfield [1999] and Chipperfield [2006]. For the simulations presented here, it was used with a horizontal resolution of  $2.8^\circ \times 2.8^\circ$  longitude by latitude, with 60 hybrid  $\sigma$ - $p$  vertical levels up to 0.1 hPa. The model meteorology, including winds, temperature, and pressure data, is taken from 6-hourly ERA-Interim analyses provided by the European Centre for Medium-Range Weather Forecasts (ECMWF) [Dee et al., 2011] and transformed onto the TOMCAT model grid using a model time step of 30 min. The TOMCAT model has been previously used for a number of studies of atmospheric composition, for example, Richards et al. [2013], Hossaini et al. [2013], and Monks et al. [2015]. TOMCAT simulations, completed using the same model version and setup used in this study, were submitted to the TransCom  $\text{CH}_4$  intercomparison [Patra et al., 2011], and TOMCAT performed well in comparison with other models and with observations when simulating tropospheric  $\text{CH}_4$ . That study covered the period 1990–2008, and although the TOMCAT model overestimated the observed interhemispheric gradient (IHG) of  $\text{CH}_4$ , it agreed to within 20% (and to within 10% for the period following 2003) and captured the mean observed atmospheric growth rate to within 1 ppb/yr. It also reproduced the observed seasonal cycle of  $\text{CH}_4$  well at a number of ground-based measurement sites. TOMCAT captured the observed latitudinal gradient of sulphur hexafluoride ( $\text{SF}_6$ ) to within 8% in all years, a performance similar to that of the other models included in the comparison, although it again overestimated the IHG compared to observations. The relatively slow interhemispheric exchange in the model implied by these results was accounted for in this study through comparison of observed and simulated  $\text{SF}_6$  concentrations.

For this study, global model simulations of  $\text{CH}_4$ , CO, and  $\text{SF}_6$  were carried out for the period 2004–2011, with 3-D concentration fields of each species saved every 6 h after 1 January 2010, and vertical profiles of each species over each of the measurement sites saved hourly. The simulated concentrations were then linearly interpolated onto the altitude and time of each observation, before data from altitudes above 4 km were discarded. This altitude was chosen as the upper limit so as to ensure that the entire planetary boundary layer was included at all times while maintaining a constant altitude range that was covered by each flight. Comparisons between the modeled and observed vertical profiles up to the maximum altitude of each individual flight (not shown) indicate that the use of this 4 km cutoff rather than the full profile does not significantly affect the results.

In order to analyze the effect of regional emissions on the observed CH<sub>4</sub> concentrations within the Amazon, we split the modeled CH<sub>4</sub> field into a “background” contribution and “regional” contributions. The background contribution is the atmospheric signal of CH<sub>4</sub> from emissions that originate outside of the South American region or originate within South America but have previously been transported away from the continent. Regional contributions are those from sources located within South America that have not yet been transported away from the continent. These regional contributions were split between those from within and from outside the Amazon Basin so that

$$C_{\text{model}} = C_{\text{bkgr}} + C_{\text{basin}} + C_{\text{SA}}$$

where  $C_{\text{model}}$  represents the total modeled atmospheric concentration of CH<sub>4</sub>,  $C_{\text{bkgr}}$  is the background contribution, and  $C_{\text{basin}}$  and  $C_{\text{SA}}$  are the contributions made by emissions from within the Amazon Basin and from South American nonbasin emissions, respectively. We define the basin as the region included in the TransCom CO<sub>2</sub> inverse modeling study as “tropical South America” [Gurney *et al.*, 2002] but with regions located north of 5°N and east of 50°W removed. The purple boundary in Figure 1a shows our definition of the basin region.  $C_{\text{basin}}$  was further split into six contributions from different emission processes as follows:

$$C_{\text{basin}} = C_{\text{basin}}^{\text{anth}} + C_{\text{basin}}^{\text{BB}} + C_{\text{basin}}^{\text{WL/R}} + C_{\text{basin}}^{\text{termite}} + C_{\text{basin}}^{\text{mudvolc}} + C_{\text{basin}}^{\text{ocean}}$$

where the terms on the right-hand side of the equation represent, in order, the contributions from within the basin from anthropogenic sources (excluding biomass burning and rice), biomass burning (BB), wetlands and rice (WL/R), termites, mud volcanoes, and oceanic emissions to atmospheric CH<sub>4</sub>.  $C_{\text{SA}}$  is similarly split into these six emission sectors. However, once contributions were transported out of the South American region defined by the red box in Figure 1a (30°W–90°W, 15°N–50°S), it was converted to the background tracer  $C_{\text{bkgr}}$  and was no longer tagged according to its source type. This allowed us to evaluate the contribution of recent, regional emissions upon atmospheric CH<sub>4</sub> within the Amazon Basin.

### 3.1. Emissions

Both the CH<sub>4</sub> and CO emission inventories used in this study were compiled by combining individual source components. Before being used in the model, all components were averaged to give monthly mean emissions on the model grid while conserving the mass of emitted species.

1. The first set of wetland and rice emissions were derived using the method of Bloom *et al.* [2012]. This is a top-down method in which satellite observations of gravity anomalies are used as a proxy for water table depth. A variable methanogen-available carbon pool is updated daily, which leads to more accurate representation of the timing of methane emissions. The satellite data cannot distinguish between microbial CH<sub>4</sub> emissions from natural wetland regions and anthropogenic microbial emissions from rice cultivation, since both come from inundated regions, and therefore, wetland and rice CH<sub>4</sub> emissions are combined in this simulation [see Bloom *et al.*, 2010, 2012]. However, the relative contribution of emissions from rice paddies in the Amazon Basin is extremely small. Yan *et al.* [2009] found that Brazilian rice paddy CH<sub>4</sub> emissions amounted to less than 0.15 Tg/yr and came mostly from nonbasin regions. The vast majority of the South American WL/R signal is therefore from natural wetland sources rather than rice paddies, especially within the Amazon Basin. WL/R emissions were derived for 2010 and 2011 for the first time for this study (i.e., as an update to Bloom *et al.* [2012], in which emissions were derived up to the end of 2009). The newly derived emission estimates are based on ERA-Interim [Dee *et al.*, 2011] surface skin temperature and the Gravity Recovery and Climate Experiment release 5 equivalent water height product [Landerer and Swenson, 2012]. The Amazonian emissions produced using this method have a seasonal cycle that peaks in March–April, when regional precipitation rates also peak [Beck *et al.*, 2005]. This inventory is henceforth referred to as BLOOM.
2. A bottom-up model was also used to estimate global wetland emissions of CH<sub>4</sub>. The Joint UK Land Environment Simulator (JULES, version 3.4.1) [Clark *et al.*, 2011] is a process-based model that simulates the Earth’s land surface in terms of carbon, water, and energy variations and includes a wetland methane flux component, based on Gedney *et al.* [2004]. The CH<sub>4</sub> flux is dependent on the available carbon substrate, temperature, and the fraction of each grid box considered to be wetland. The version of JULES used here derives wetland fraction using the latest version of the TOPography-based hydrological MODEL

**Table 1.** Sources and Sinks of CH<sub>4</sub> Used in This Study, and the Basin-Wide Total Emissions From Each Source Type for the Years 2010 and 2011 (Tg(CH<sub>4</sub>)/yr)

Emission Type	Taken From the Following:	Annually Varying?	Basin Total (2010, Tg(CH <sub>4</sub> )/yr)	Basin Total (2011, Tg(CH <sub>4</sub> )/yr)
Wetlands and rice (1)	<i>Bloom et al.</i> [2012]	Yes	19.5	20.8
Wetlands (2)	JULES wetland model [ <i>Clark et al.</i> , 2011]	Yes	20.4	20.8
Rice (2)	<i>Yan et al.</i> [2009]	No	0.2	0.2
Biomass burning	GFED v3.1 [ <i>van der Werf et al.</i> , 2010]	Yes	5.4	0.5
Anthropogenic	EDGAR database (v3.2) [ <i>Olivier and Berdowski</i> , 2001]	No	5.3	5.3
Termites	<i>Matthews and Fung</i> [1987]	No	2.0	2.0
Mud Volcanoes	<i>Etiopie and Milkov</i> [2004]	No	0.2	0.2
Oceanic	<i>Lambert and Schmidt</i> [1993]; <i>Houweling et al.</i> [1999]	No	0.01	0.01
Soil sink	<i>Bousquet et al.</i> [2006]	No	-0.2	-0.2

(TOPMODEL) described in *Marthews et al.* [2015], and produces significantly lower methane emissions from Amazon Basin region than the model did when using previous versions of TOPMODEL. Basin-wide emissions peak in March–April, similarly to the BLOOM inventory, although the magnitude of the seasonal cycle is approximately 50% smaller in JULES. The model uses WATCH meteorological forcing data, and global wetland emissions were scaled to give mean total emissions of 175 Tg CH<sub>4</sub>/yr over the period 1993–2012, the global total taken from *Ciais et al.* [2013].

- Since the JULES model does not simulate CH<sub>4</sub> emissions from agricultural rice farming, we include a separate tracer for these emissions when using JULES. Here rice emissions are taken from *Yan et al.* [2009] and are scaled as in *Patra et al.* [2011] to give total global emissions of approximately 39 Tg CH<sub>4</sub>/yr.
- Anthropogenic emissions were taken from the Emission Database for Global Atmospheric Research (EDGAR) v3.2 inventory [*Olivier and Berdowski*, 2001]. The combination of different anthropogenic emission categories and the interpolation/extrapolation of EDGAR emission maps provided for the years 1990, 1995, and 2000 are described in *Patra et al.* [2009] and give almost constant global anthropogenic emissions (~259 Tg/yr) after 2000. While it is unlikely that this was the case, the updated EDGAR v4.0 (<http://edgar.jrc.ec.europa.eu>) inventory has been shown to lead to significant overestimation compared to the observed CH<sub>4</sub> growth rate in the 2000s when used in models, while simulations using v3.2 were shown to agree better with observations up to 2008 [*Patra et al.*, 2011]. Despite the fact that the continued increase in global CH<sub>4</sub> concentrations since 2008 may not reconcile with static anthropogenic emission totals, it was decided that the earlier emission data set would be used in this study. It should, however, be noted that the relative contribution of anthropogenic sources to CH<sub>4</sub> concentrations in our model simulations may be too small.
- Biomass burning emissions come from the the Global Fire Emissions Database (GFED) v3.1 data set [*van der Werf et al.*, 2010], which uses remote sensing methods in order to estimate burned area and a land vegetation model to calculate fuel loads.
- Emissions due to oceanic exchange are distributed over the coastal region [*Lambert and Schmidt*, 1993; *Houweling et al.*, 1999], and mud volcano emissions are based upon *Etiopie and Milkov* [2004]. Emissions from termites were taken from the GISS inventory [*Matthews and Fung*, 1987; *Fung et al.*, 1991].
- A sink due to the consumption of atmospheric methane by methanotrophs within the soils was also included. This soil sink does not vary annually, but does have a small seasonal cycle, and was obtained from the LMDZ atmospheric CH<sub>4</sub> inversion [*Bousquet et al.*, 2006]. The basin contribution to the global soil sink is small (<1%).

Further details of the emission inventories used in this study, along with their total contributions to the basin-wide surface flux of CH<sub>4</sub>, are given in Table 1. Figure 1 shows the seasonal mean basin-wide WL/R emissions for January 2010 to March 2010 (the “wet season,” January–March, JFM) and July–September 2010 (the “dry season,” July–September, JAS), and the changes to these emissions 1 year later, along with the mean BB emissions for JAS 2010. BB emissions in 2011 were relatively insignificant and are not shown.

The inventories produced by the two wetland models have a similar geographical distribution of CH<sub>4</sub> emissions in and around the basin in 2010. In both models, there are significant WL/R emissions toward the northern and southern sides of the basin in JFM 2010, but by the following dry season, JAS 2010, the southernmost emissions decrease significantly, while the emissions to the north of the basin increase slightly.

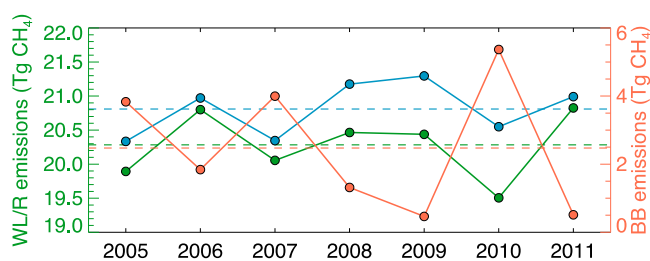


**Figure 3.** Total basin-wide annual wetland and rice (WL/R, left axis) using the method of Bloom *et al.* [2012] (green) and JULES land surface model (blue), and biomass burning (BB, right axis and red line) [van der Werf *et al.*, 2010] emission estimates of methane (Tg(CH<sub>4</sub>)/yr) for the period 2004–2011. The dotted lines indicate the average annual emissions for each source type over this period.

Basin-wide emissions are smaller overall during the dry season. In both seasons, the emissions in JULES are redistributed more toward the north of the continent in comparison with the BLOOM inventory. In 2011, which was a much wetter year than 2010 (see Figure 2), the two models display somewhat contrasting behaviors. The WL/R emissions of the BLOOM inventory increase almost everywhere throughout the basin in 2011 compared to those of 2010, especially during the wet season (although some individual grid cells do display decreased emissions). The

JULES inventory, however, displays more geographically diverse changes between the two years. In JFM 2011, there are significantly larger emissions to the north and southeast of the basin than in JFM 2010, while emissions from within the basin decrease slightly. In the dry season of 2011, however, there is not much change from the previous year's dry season, although emissions do increase slightly across the south. In both cases, annual emissions from the basin are larger in 2011 than in 2010, as expected due to the increased precipitation (see Table 1).

Biomass burning (BB) emissions in JAS 2010 were large across much of the south of the basin, a region that generally experiences high rates of deforestation [van der Werf *et al.*, 2010]. Aragão *et al.* [2008] showed that drought events such as the one that occurred in 2010 can significantly increase fire occurrence in the Amazon Basin even in years with lower rates of deforestation, however. The southernmost measurement sites in the study (RBA and ALF) are situated near areas displaying large BB emissions and so are expected to be particularly affected by these emissions.

Figure 3 shows the total annual basin emission estimates for WL/R and BB for the period 2004–2011. The wetland emissions and biomass burning emissions are strongly anticorrelated (BLOOM:  $r = -0.89$ , JULES:  $r = -0.79$ ), due to the opposing effect of precipitation on the rate of emission from the two source types [e.g., Bloom *et al.*, 2010; van der Werf *et al.*, 2010], with both 2010 and 2011 displaying particularly significant deviations from the 8 year average in the BLOOM WL/R inventory and the BB emissions. Basin-wide BLOOM WL/R emissions over 2004–2011 vary between 19.5 and 20.8 Tg(CH<sub>4</sub>)/yr, JULES WL/R emissions vary between 20.3 and 21.4 Tg(CH<sub>4</sub>)/yr, while BB emissions ranged between 0.4 and 5.4 Tg(CH<sub>4</sub>)/yr. BLOOM WL/R emissions vary relatively little around the mean ( $\sigma^2 = 0.45$  Tg(CH<sub>4</sub>)/yr), but 2010 has the smallest total emissions over the 8 year period (19.5 Tg(CH<sub>4</sub>)/yr), while 2011 has the largest (20.8 Tg(CH<sub>4</sub>)/yr). JULES WL/R varies even less than BLOOM around the mean emission value ( $\sigma^2 = 0.40$  Tg(CH<sub>4</sub>)/yr) but has a larger positive trend over the time period than that of the BLOOM WL/R emissions. The years 2010 and 2011 are not particular outliers from the mean over the period in this inventory. The GFED BB emissions vary significantly year on year, with particularly large (small) emissions in 2010 (2011), suggesting that combustion emissions are much more sensitive than microbial WL/R emissions to variations in temperature and precipitation. These differences caused by the meteorological regimes over the basin allow us to assess the effect of the drought on regional atmospheric CH<sub>4</sub> concentrations.

CO emissions were treated as in Monks *et al.* [2012]. Anthropogenic emissions were taken from the IPCC AR5 anthropogenic estimates for the year 2000 [Lamarque *et al.*, 2010], while the direct natural CO emissions were taken from the POET database [Olivier *et al.*, 2003]. BB CO emissions were taken from the GFED v3.1 data set [van der Werf *et al.*, 2010] and are therefore comparable with the CH<sub>4</sub> BB emission tracer. We included secondary production of CO from anthropogenic and biomass burning emitted hydrocarbons by scaling the corresponding emissions of CO upward by 18.5% and 11%, respectively, following Duncan *et al.* [2007]. Production of atmospheric CO from biogenic emissions of isoprene (C<sub>5</sub>H<sub>8</sub>) was accounted for by scaling the global 568 Tg (C<sub>5</sub>H<sub>8</sub>)/yr emissions of isoprene to give 127 Tg(CO)/yr, according to the assumption that C<sub>5</sub>H<sub>8</sub> is oxidized immediately to give CO, also as in Duncan *et al.* [2007]. In order to account for secondary production of CO by CH<sub>4</sub> oxidation, a climatological monthly mean 3-D CH<sub>4</sub> field from a previous TOMCAT simulation and

**Table 2.** Sources and Sinks of CO Used in This Study, and the Total Basin-Wide Emissions From Each Source Type for the Years 2010 and 2011 (Tg(CO)/yr)

Emission Type	Taken From the Following:	Annually Varying?	Basin Total (2010, Tg(CO)/yr)	Basin Total (2011, Tg(CO)/yr)
Anthropogenic	IPCC AR5 [Lamarque <i>et al.</i> , 2010], increased by 18.5% to account for hydrocarbon oxidation.	No	3.3	3.3
Biomass burning	GFED v3.1 [van der Werf <i>et al.</i> , 2010], increased by 11% to account for hydrocarbon oxidation.	Yes	96.1	9.3
Isoprene	Isoprene emissions calculated by MEGAN model [Guenther <i>et al.</i> , 2006] and scaled to give CO (as in Duncan <i>et al.</i> [2007]).	No	26.8	26.8
Direct natural	POET database [Olivier <i>et al.</i> , 2003; Granier <i>et al.</i> , 2005]	No	15.0	15.0

climatological monthly mean OH fields (described in the following section) were used to estimate atmospheric CO production, under the assumption that one molecule of CH<sub>4</sub> gives one molecule of CO when reacting with OH. Further details of CO emissions are given in Table 2.

SF<sub>6</sub> emissions for the period were derived using a similar method to that of Levin *et al.* [2010], where total surface fluxes of SF<sub>6</sub> are inferred from estimations of changes to the total global atmospheric SF<sub>6</sub> budget. We used the combined global SF<sub>6</sub> concentration data provided by the Halocarbons and other Atmospheric Trace Species Group as part of the NOAA/ESRL measurement network, which is derived from a global network of flask and in situ measurements. Using this data to find the annual mean increase in the atmospheric SF<sub>6</sub> budget, we applied scaling factors to the EDGAR v4.0 distribution of SF<sub>6</sub> emissions for 2005. SF<sub>6</sub> is emitted almost entirely from anthropogenic sources, meaning that the geographical distribution of the surface flux of the species is well understood [Levin *et al.*, 2010]. The global SF<sub>6</sub> emissions that we derived using this method were approximately 7.8 Gg SF<sub>6</sub>/yr in both 2010 and 2011.

### 3.2. Chemistry

The chemical destruction of CH<sub>4</sub> in the atmosphere was treated as in Patra *et al.* [2011]. Three-dimensional monthly mean climatological OH fields were provided for online calculation of CH<sub>4</sub> loss in the model and were produced by combining semiempirically calculated tropospheric distributions [Spivakovsky *et al.*, 2000] with two-dimensional (2-D) model simulated stratospheric output. The OH fields were then uniformly reduced by approximately 8% in order to match atmospheric loss rates of methyl chloroform (MCF, CH<sub>3</sub>CCl<sub>3</sub>) [Huijnen *et al.*, 2010]. The loss of CH<sub>4</sub> was then determined using the kinetic loss rate of

$$k_{\text{CH}_4+\text{OH}} = 2.45 \times 10^{-12} \exp(-1775/T) \quad (\text{R1})$$

where  $T$  is temperature (K) and  $k$  has units of cm<sup>3</sup> molecule<sup>-1</sup> s<sup>-1</sup>, as used in Patra *et al.* [2011]. Reaction (R1) was also used to provide the chemical source of CO from CH<sub>4</sub>. For CH<sub>4</sub> reactions with Cl and O(<sup>1</sup>D) radicals in the stratosphere, parameterized loss rates were based on the Cambridge 2-D model [Velders, 1995], also as in Patra *et al.* [2011]. Reaction rates are taken from Sander *et al.* [2006]. The climatological OH fields were also used in order to calculate atmospheric CO loss in the model, using the kinetic loss rate

$$k_{\text{CO}+\text{OH}} = 1.44 \times 10^{-13} (1 + [\text{N}_2]/4.2 \times 10^{19}) \quad (\text{R2})$$

where [N<sub>2</sub>] is the atmospheric concentration of nitrogen gas (N<sub>2</sub>, molecules cm<sup>-3</sup>) as used in Monks *et al.* [2012].

SF<sub>6</sub> is inert in the troposphere and stratosphere and had no atmospheric sinks included in the simulations. A constant offset was applied to the global SF<sub>6</sub> concentration by removing the mean model-observation bias in January 2010 at the South Pole NOAA/ESRL station (90.0°S) (approximately 0.12 parts per trillion, ppt).

### 3.3. SF<sub>6</sub>-Based Correction of Background CH<sub>4</sub>

In order to remove any initial bias between the modeled and observed CH<sub>4</sub> concentration, a constant offset of 10 ppb was added to the simulated background CH<sub>4</sub>. This value was chosen to match the mean

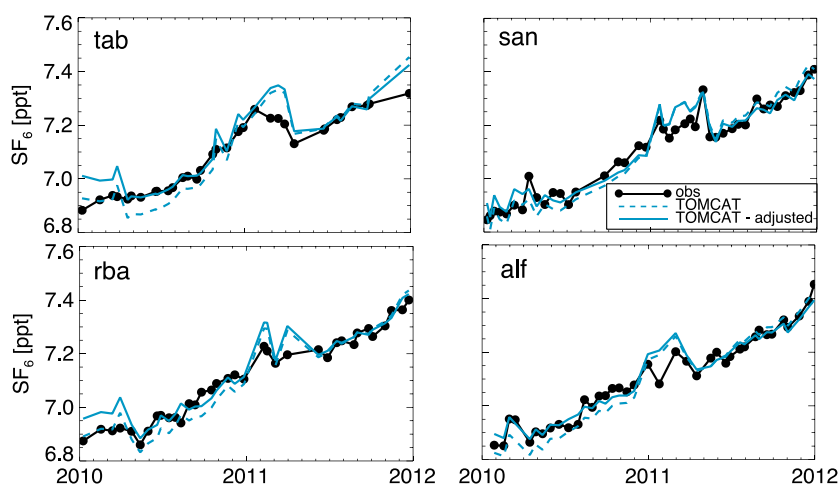


**Figure 4.** Observed (black lines) and simulated (blue lines) mean (below 4 km) SF<sub>6</sub> concentrations (ppt) at four Amazon Basin sites for the years 2010 and 2011. Dashed blue line shows standard model SF<sub>6</sub> concentrations, while solid blue line shows readjustment of model SF<sub>6</sub> using the observed trend at each site, as explained in the main text.

concentration of all observations made at the remote station at Ragged Point, Barbados (RPB, 59.4°W, 13.2°N), in January 2010 as part of the NOAA/ESRL observation network. RPB is located to the north of the Amazon Basin, and the air sampled there is therefore representative of the background CH<sub>4</sub> concentration. After applying this constant offset, the model captures the observed variation at RPB throughout 2010 and 2011 fairly well when using both of the wetland emission inventories included in the study (BLOOM:  $r^2 = 0.44$ ,  $p < 0.01$ , mean bias =  $-10.1$  ppb; JULES:  $r^2 = 0.52$ ,  $p < 0.01$ , mean bias =  $-4.5$  ppb; see supporting information), although the JULES inventory captures the small positive trend better than the BLOOM inventory does. In both cases, however, the observed trend at RPB is larger than the simulated trend. This may lead to overestimation of basin-wide emissions in 2011 in our analysis, having a larger effect when using the BLOOM inventory than the JULES inventory, and it should therefore be noted that the emission estimates provided in this work may be artificially high. No offset was applied to simulated CO.

In order to accurately assess the effect of only local and regional emissions of CH<sub>4</sub> within Amazonia, it is vital to obtain an accurate estimation of the background CH<sub>4</sub> concentration at the sites. While TOMCAT model simulations of CH<sub>4</sub> generally perform well in comparison with observations [Patra *et al.*, 2011], it has been suggested that the interhemispheric transport in the model is a little slow, and if so, this will affect the model's performance at SH sites like those in the Amazon Basin. Here we used the observed SF<sub>6</sub> concentrations at the Amazon sites to correct the model transport of background air and therefore improve the simulated background CH<sub>4</sub> concentrations. Figure 4 shows the modeled and observed mean SF<sub>6</sub> concentrations below 4 km at each of the sites for 2010 and 2011. While the model generally captures the observed growth rate and timing of the large-scale variations at the sites well, there are sometimes significant errors between the observed and simulated values. The model-observation mismatch is likely to stem from transport errors in the model, with the movement of the ITCZ playing an important role in the seasonal variation of SF<sub>6</sub> and CH<sub>4</sub> at these sites. In addition, the simulated trend in SF<sub>6</sub> is slightly larger in the model than the observed trend. Since the SF<sub>6</sub> emissions used in the model are based on the observed atmospheric growth rate, this is also likely due to model transport errors.

Here we describe our method of correcting the simulated background CH<sub>4</sub> concentrations using the discrepancies between the observed and simulated SF<sub>6</sub> concentrations. At each site, we altered the linear trend of the simulated SF<sub>6</sub> concentrations to match that of the observations at that site. Both the simulated and observed linear trends were derived only from the concentrations during May–September, which were assumed to be representative of the Southern Hemisphere SF<sub>6</sub> trend. Next, we extracted the latitudinal distribution of simulated SF<sub>6</sub> and background CH<sub>4</sub> at the longitude of each Amazon site at the time that each flight at that site was undertaken. Making the assumption that the model-observation SF<sub>6</sub> error at each site was due only to errors in the north-south ITCZ movement, we found the latitude at which the model SF<sub>6</sub> concentration

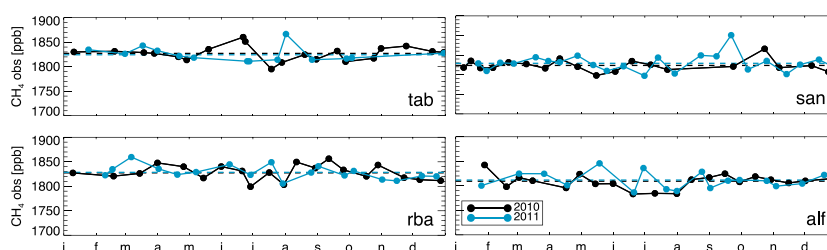


**Figure 5.** Observed mean (below 4 km) CH<sub>4</sub> (ppb) at four Amazon Basin sites for the years 2010 (black) and 2011 (blue). Mean annual concentrations at each site are shown as dashed lines.

matched the observed one. Finally, we extracted the CH<sub>4</sub> background concentration at this new latitude as the “SF<sub>6</sub>-based background CH<sub>4</sub> concentration.” This method of finding the background concentrations of CH<sub>4</sub> has the advantage that it is based on observed variations of atmospheric transport. Disadvantages include the assumption that all SF<sub>6</sub> errors are due to transport errors along a latitudinal axis and are not subject to errors in longitudinal and vertical transport. This method also assumes that there are no errors in CH<sub>4</sub> emissions from other tropical regions that affect the Amazonian sites, mainly from Africa. Corrections of up to 50 ppb are made to the background CH<sub>4</sub> concentration using this method, although changes are generally between 10 ppb and 20 ppb. The main features of the SF<sub>6</sub>-based background are a less-pronounced seasonal cycle in 2010 than in the standard model background and a much shorter influence of NH air during into beginning of 2011 than that provided by the standard model (see Figures 6 and 7).

## 4. Results and Discussion

### 4.1. Spatial and Temporal Variation of Amazon CH<sub>4</sub>

The observed data together with the model simulations allow us to analyze the temporal and spatial variation of Amazon CH<sub>4</sub> throughout 2010 and 2011. Figure 5 shows the observed ( $\leq 4$  km mean) CH<sub>4</sub> concentrations at each site for 2010 and 2011. Although each site displays a distinct pattern of temporal variation and no site displays an obvious seasonal cycle, the majority of the enhancements to CH<sub>4</sub> concentration generally occur between March and October. Monthly mean concentrations were found at each location and were then used to derive annual means. If, in either year, there was a month in which no flights were undertaken, that month was not included in the annual mean for either of the years so that they would be comparable. The change to the annual mean CH<sub>4</sub> concentration between 2010 and 2011 displays little consistency between the different measurement sites, and the relatively small number of measurements makes it difficult to assess the significance of the changes. At SAN, the annual mean concentration rises by 5.5 ppb in 2011 compared to 2010, while there is a 2.5 ppb increase at ALF. However, there is no change in annual mean concentration at RBA, and TAB displays a 2.8 ppb decrease in 2011 compared to 2010. While these mean concentrations are likely to be affected by the relatively low temporal resolution at which the observations are made, meaning that the year-on-year changes are insignificant at all sites ( $p > 0.05$ ), they indicate that there may have been slightly larger CH<sub>4</sub> concentrations over the eastern site of the basin (affecting SAN and ALF) in 2011 than in 2010. The western basin, however, may have experienced little change or even a slight decrease in concentrations during 2011. Globally, the mean atmospheric CH<sub>4</sub> growth rate was approximately 5–6 ppb between 2010 and 2011 [McNorton *et al.*, 2016], so concentrations at three of the basin sites appear to have experienced significantly less growth than the global average. At all sites, the values of minimum concentrations are almost identical in 2010 and 2011, while the timing and magnitude of CH<sub>4</sub> enhancements varies in each year. This means either that there is little change to the background methane concentration or to the regional emissions, or that both the background concentration, and the regional emissions have changed in opposing directions so as to produce little overall variation.

The tagged model simulations allow us to evaluate the effect that background CH<sub>4</sub> variations had at each of the sites. Observed and modeled mean CH<sub>4</sub> concentrations are shown in Figures 6 and 7. In order to investigate the effect of only South American CH<sub>4</sub> emissions at each site, the standard modeled background CH<sub>4</sub> concentrations have been subtracted both from the modeled and observed total CH<sub>4</sub>, leaving the modeled and observed “regional contributions.” Also shown are the SF<sub>6</sub>-based modeled background CH<sub>4</sub>

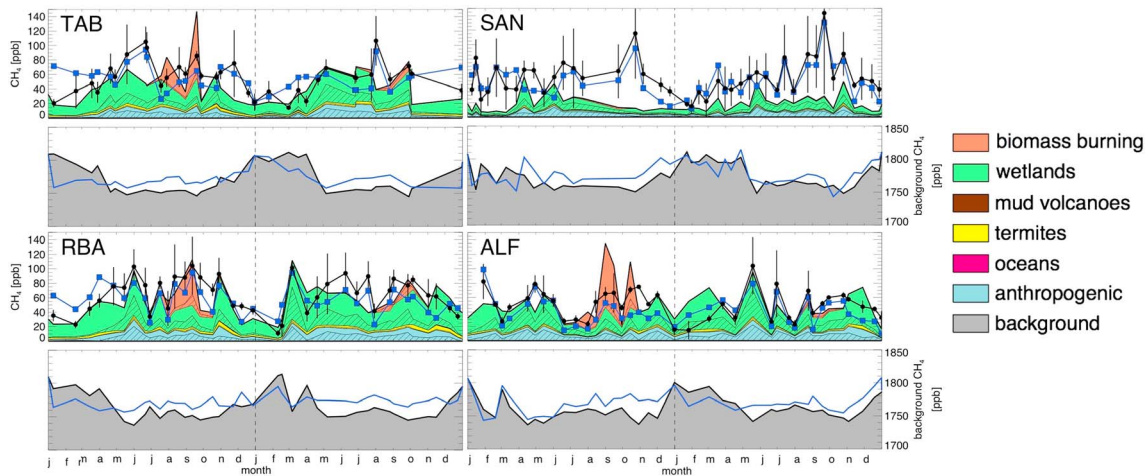


**Figure 6.** Observed and simulated mean (below 4 km) CH<sub>4</sub> with simulated and SF<sub>6</sub>-based background CH<sub>4</sub> subtracted (ppb, rows 1 and 3) and simulated (below 4 km) mean and SF<sub>6</sub>-based background CH<sub>4</sub> (ppb, rows 2 and 4) at four Amazon Basin sites for the years 2010 and 2011. Wetland emissions calculated using the method of Bloom *et al.* [2012]. Observations are shown as black circles (using standard model background) or blue squares (using SF<sub>6</sub>-based background), with vertical black lines signifying 1σ of the observations within each vertical profile. Solid color blocks represent simulated CH<sub>4</sub> emitted within South America, tagged according to emission type. Unhatched colored sections indicate CH<sub>4</sub> emitted within the Basin, while hatched sections represent CH<sub>4</sub> emitted in non-Amazonian South America. Standard modeled background CH<sub>4</sub> is shown in gray; SF<sub>6</sub>-based background CH<sub>4</sub> is indicated by blue solid lines.

concentrations and the equivalent observed regional contribution of CH<sub>4</sub>, found by subtracting the SF<sub>6</sub>-based concentration from the observed values. Across the sites, South American emissions of CH<sub>4</sub> contribute up to 150 ppb to the observed total concentration. The performance of the two WL/R inventories is similar, with  $r^2$  values between the two simulated regional contributions at each site being greater than 0.85 (and > 0.96 at ALF and SAN). Simulated South American contributions to CH<sub>4</sub> at ALF, TAB, and RBA compare well with the observations using both WL/R inventories (mean bias (MB) of 4.9, -8.9, and -2.9 ppb, respectively, using BLOOM; MB = -7.4, -9.4, -7.3 ppb, respectively, using JULES) and track the observed time variation in CH<sub>4</sub> fairly well (BLOOM  $r^2$  = 0.34, 0.28, 0.63; JULES  $r^2$  = 0.33, 0.30, 0.49,  $p < 0.01$  in all cases), although there are often instances when the observed methane concentration is significantly underestimated or overestimated in the model. Introducing the SF<sub>6</sub>-based background concentration significantly diminishes the model performance at each station (MB = 9.9, -12.3, -2.0 ppb using BLOOM, MB = -2.5, -13.1, -5.5 ppb using JULES; BLOOM  $r^2$  = 0.11, 0.03, 0.22; JULES  $r^2$  = 0.12, 0.0, 0.19; all correlations insignificant at  $p < 0.01$ ). This suggests that the assumptions that our SF<sub>6</sub> adjustment method is based upon may be incompatible with

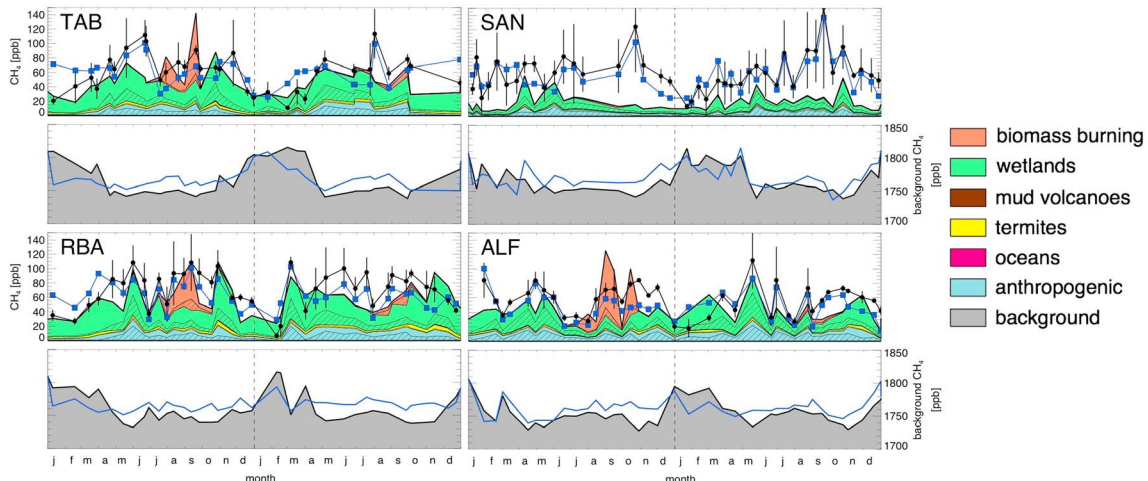


**Figure 7.** As Figure 6, but using JULES wetland emissions.

the atmospheric model transport and/or the emission inventories. However, the use of this method provides an indication of the influence of model transport uncertainty on the comparisons and our estimates of methane emissions from within the basin.

At SAN, the observed enhancements from South American emissions were often larger than 100 ppb, with a maximum regional contribution of up to 150 ppb in September 2011. Enhancements of this magnitude were not observed at any of the other locations. Since observations made at SAN sample only a small proportion of the basin, this might indicate significant local emissions that were dispersed by the time they reach the other sites or possibly more elevated background concentrations than at the other measurement locations, which were not captured by the model. The large standard deviation displayed by many of the observations at SAN is due to significantly larger concentrations in the boundary layer than in the free troposphere (not shown), which is indicative of large local emissions. Here, unlike at the other sites, simulated CH<sub>4</sub> does not capture the magnitude of the observed concentrations (MB = -43.2 - -31.7 ppb). Simulated CH<sub>4</sub> concentrations at SAN are not significantly affected by contributions from South American emissions, which provide as little as 10 ppb and a maximum of 55 ppb to the total. This leads us to suggest that there are significant but localized recurrent fluxes of CH<sub>4</sub> near SAN that are not currently included in the emission inventories used in this study.

At all four sites, the standard model background CH<sub>4</sub> concentration generally varies between 1750 and 1830 ppb and displays a marked seasonal cycle, increasing during the boreal winter as the intertropical convergence zone (ITCZ) moves south of the equator. As the ITCZ moves south, the air samples taken within the basin are likely to contain a larger contribution from the Northern Hemisphere (NH) than samples taken when the ITCZ is further north. The seasonal cycle is significantly less pronounced in the SF<sub>6</sub>-based background concentrations, however. According to the standard model background, the seasonal influence of NH background air lasts longer in 2011 than in 2010, especially at the two northern locations. *Marengo et al.* [2011] showed that during early 2010 sea surface temperatures in the tropical North Atlantic Ocean were anomalously high, which has been shown to be associated with a more northward shift in the position of the ITCZ during NH spring [*Li et al.*, 2006; *Malhi et al.*, 2008; *Zeng et al.*, 2008]. Increased tropical North Atlantic SST has also been linked to droughts within the basin in 2005 and 2010 among other years [*Lewis et al.*, 2011]. The SF<sub>6</sub>-based background concentrations do not display the same prolonged influence of the ITCZ in 2011 as seen in the standard model. At TAB in particular, the standard model significantly overestimates the concentration of background CH<sub>4</sub> in early 2011 compared to the SF<sub>6</sub>-based background. The reduction of background CH<sub>4</sub> concentrations at the start of each year when applying the SF<sub>6</sub> correction implies larger regional emissions during January–April than those indicated by the standard model background concentrations.

Both the standard and the SF<sub>6</sub>-based model background CH<sub>4</sub> display increased annual mean concentrations in 2011 compared to 2010. Apart from the standard model mean background concentration at RBA, which increases by less than 1 ppb when using either WL/R inventory, each site displays an increase of between 4 ppb and 9 ppb. This is comparable to the global growth rate of approximately 6 ppb across the two years. This leads us to suggest that the relatively stable observed concentrations at the sites is due to decreased emissions in 2011 compared to 2010, which cancel the effect of increasing background concentrations.

#### 4.2. Source Attribution of Amazon CH<sub>4</sub>

At ALF, TAB, and RBA, emissions from WL/R sources give the largest contribution (12–87%) throughout the period, with smaller contributions from anthropogenic sources and, to a much lesser degree, termites. Emissions from biomass burning sources make significant contributions during 2010 but contribute only very little in 2011. Unsurprisingly, the majority of the anthropogenic contribution originates outside of the basin (indicated by hatched sections), while WL/R and BB sources are largely contained within the basin (unhatched sections). However, the relative contribution of basin and nonbasin emissions varies with time. Generally, the influence of nonbasin South American emissions is larger in the dry season than the wet season. At the western sites (RBA and TAB) especially, the nonbasin South American contribution is almost zero during each wet season.

Depending on whether the standard or SF<sub>6</sub>-based background is used, the model either captures or overestimates the regional contribution of BB sources to a small extent during the dry season of 2010 at RBA. However, the model significantly overestimates the regional contribution at this time (by up to 80 ppb) at

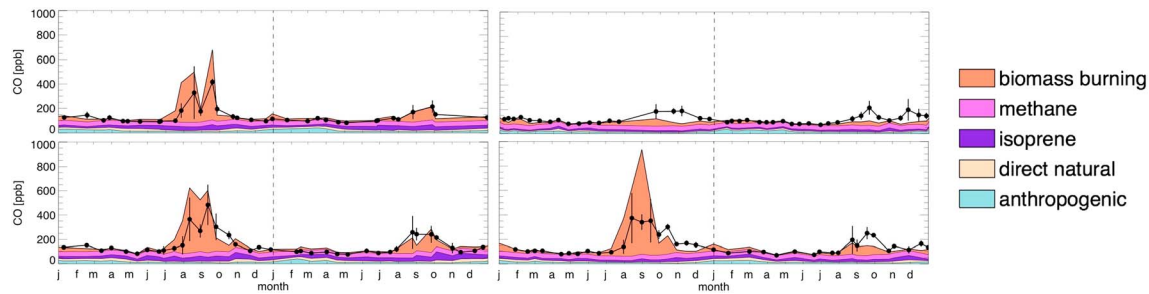


**Figure 8.** Observed and simulated mean (below 4 km) CO at four Amazon Basin sites for the years 2010 and 2011. Observations are shown as black circles with vertical black lines signifying  $1\sigma$  of the observations. Solid color blocks represent simulated CO emitted within South America, tagged according to emission type, but with no separation by emission location.

TAB and particularly at ALF, mainly due to a significant contribution from BB emissions. ALF is located closest to the region of significant BB emissions (see Figure 1), and it appears either that the magnitude of these emissions is overestimated or that the model's representation of transport to this site is inaccurate. One possibility is that due to the model's horizontal grid resolution of  $2.8^\circ$ , there is a numerical diffusion effect that is artificially spreading the BB emissions toward the site, although since each of the surrounding model grid boxes contains similarly high concentrations from BB emissions (not shown), this is unlikely. *Bloom et al.* [2015] compared basin-wide carbon emissions during the dry seasons of 2007 and 2010 and found that despite total burned area within the basin being similar in these two years, it was extremely likely that a reduction in biomass combustion rates in 2010 contributed to smaller total carbon fire emissions. Also, increased combustion efficiency in the region in 2010 was a smaller contributing factor to reduced emissions of CO (and likely also  $\text{CH}_4$ ). The performance of the GFED inventory in our simulations suggests that the methodology used to derive  $\text{CH}_4$  and CO emissions in the inventory may not have fully taken account of the changes to combustion rates and efficiency in 2010.

The modeled and observed CO concentrations allow us to examine the effect of BB emissions on the sites, since CO is a good tracer of these combustion emissions (e.g., *Monks et al.* [2015]). Figure 8 shows the observed and simulated mean concentrations of CO at each of the four sites. As with  $\text{CH}_4$ , the measurements made at TAB, RBA, and ALF display higher concentrations due to BB emissions in 2010 than in 2011. The model captures the timing of the observed variations well, with high correlations at each of these three sites ( $r^2 > 0.8$ ). However, the effect of BB emissions in the simulations is too large at TAB, RBA, and ALF (where the model overestimates the observed concentrations by up to 500 ppb) in 2010. Assuming that the relative emission factors used to compile the  $\text{CH}_4$  and CO BB emissions are correct [*van der Werf et al.*, 2010], it is therefore likely that the contribution of BB emissions to the simulated  $\text{CH}_4$  concentration at these sites is also overestimated. Again, it is difficult to ascertain whether this is due to errors in the magnitude and location of the BB emissions or in the model transport.

As with  $\text{CH}_4$ , the observations of CO made at SAN display different behavior compared to the other three locations, as the site is not significantly affected by biomass burning emissions. CO concentrations at the site are therefore much smaller than at any of the other locations. The observations at SAN indicate enhancements of 100–200 ppb toward the end of each year that are not captured in the model and are not seen at the other sites, which may be due to relatively small local biomass burning or anthropogenic sources that are not included in the model emission inventories. The fact that these enhancements occur during the end of the basin-wide fire season in September to November indicates that they may be most likely from BB sources. *Kaiser et al.* [2012] showed that the GFED v3.1 inventory underestimates combustion emissions in some regions due to the missed contribution of undetected small fires. The relatively small enhancements of CO at SAN (compared to those at other sites) can provide some information about the nature of the significant enhancements of observed  $\text{CH}_4$  at the same site. Atmospheric CO concentrations are generally more readily affected by BB sources than  $\text{CH}_4$  concentrations, and it is therefore likely that if the  $\text{CH}_4$  enhancements observed at SAN came from combustion sources, we would also expect to see significantly enhanced CO concentrations at the same time. Also,  $\text{CH}_4$  enhancements at SAN occur frequently throughout each year, while the timing of the CO enhancements is toward the end of each year. The lack of correlation between CO and

**Table 3.** Total Basin-Wide Emissions (Tg (CH<sub>4</sub>), All Sources) for the Years 2010 and 2011 Before and After Optimal Scaling Factors  $\lambda^{SA}$  and  $\lambda^{BB}$  Are Applied to the Prior Emissions<sup>a</sup>

Year	WL/R Used	Prior Emissions (All Sources, Tg-CH <sub>4</sub> )	Posterior Emissions (All Sources, Tg-CH <sub>4</sub> , Standard Model Background)	Posterior Emissions (All Sources, Tg-CH <sub>4</sub> , SF <sub>6</sub> -Based Background)
2010	BLOOM	32.3	38.7	41.1
	JULES	33.4	36.5	40.7
2011	BLOOM	28.8	32.1	37.9
	JULES	29.0	31.6	38.8

<sup>a</sup>Emissions are calculated using two wetland emission estimates (Bloom and JULES) and two simulated background CH<sub>4</sub> concentrations (standard and SF<sub>6</sub> based).

CH<sub>4</sub> concentrations at SAN therefore indicates that the large CH<sub>4</sub> enhancements at SAN are more likely to be a result of elevated local emissions from microbial sources than from combustion sources.

### 4.3. Amazon CH<sub>4</sub> Balance and Comparison With Existing Estimates

Together, the observations and model simulations of CH<sub>4</sub> allow us to draw conclusions about Amazonian Basin CH<sub>4</sub> emissions. The greatest uncertainty surrounding emissions from South America concerns the magnitude, distribution, and timing of wetland emissions. The generally small mean biases between the simulated and observed concentrations at three of the sites therefore indicates that the total annual basin-wide emissions of 32.3–33.4 Tg/yr in 2010 and 28.8–29.0 Tg/yr in 2011 that were used in the model can broadly reproduce the mean observed atmospheric signal. Mean absolute model biases at each site over the period are smaller than 10 ppb when using the standard model background CH<sub>4</sub> and below 14 ppb when using the SF<sub>6</sub>-based background concentrations. Generally, the simulated values are lower than the observed concentrations at the western sites and are too high at ALF, indicating that total prior emissions may be too low and that the geographical distribution of emissions or the model transport is incorrect. In order to further evaluate the accuracy of the emissions, we estimated optimal scaling factors ( $\lambda$ ) to the South American biomass burning emissions ( $\lambda^{BB}$ ) and to the remaining South American emissions ( $\lambda^{SA}$ ) for 2010 and 2011 in order to minimize a weighted-mean bias between the model and the observations at TAB, RBA, and ALF, where ALF was giving a weighting one third that of RBA and TAB, since it samples air representative of a much smaller proportion of the basin [Gatti *et al.*, 2014]. Observations made at SAN sample air that is representative of a relatively small proportion of the Amazon Basin and are therefore disproportionately affected by localized emissions, so these were not used in order to derive scaling factors. In order to reduce the effect of observations made within a short time of each other, observed and modeled concentrations were binned to create monthly mean values, before each  $\lambda$  was found as a weighted average of the individual scaling factors. We used only CO concentrations during June–September in order to find an independent  $\lambda^{BB}$  for each year. Assuming the relative burning emission factors for CO and CH<sub>4</sub> are correct, we then applied  $\lambda^{BB}$  to the South American CH<sub>4</sub> biomass burning emissions and used the rescaled simulated concentrations to find  $\lambda^{SA}$  for each 3 month period during 2010 and 2011. This is a relatively simple way of finding an optimum scaling factor to apply to the emissions, and it makes the assumption that the background CH<sub>4</sub> is correct and that the difference between the model output and the observations are therefore due only to errors in the South American emissions. It also does not allow for any geographical redistribution of the emissions and assumes a linear relationship between emissions and concentrations in each 3 month period, without allowing correlations between time periods. However, it provides a first assessment of the model's accuracy against observations without the need for a more complex inverse modeling method, which may be used in the future in order to better constrain the emissions. The results of this scaling are summarized in Table 3. Figure 9 shows the seasonal CH<sub>4</sub> bias between the model and the observations at each measurement site before and after the scaling factors have been applied.

We find that our prior estimate of BB emissions decreases by 42% in 2010 and increases by 30% in 2011 in order to minimize the mean bias between simulated and observed CO concentrations. Applying these scaling factors to our prior CO and CH<sub>4</sub> emissions gives total combustion emissions of 55.7 Tg CO and 3.1 Tg CH<sub>4</sub> in 2010, and 11.6 Tg CO and 0.6 Tg CH<sub>4</sub> in 2011. These scaling factors imply that total BB emissions in Amazonia in 2011 were approximately 20% of those emitted in 2010, rather than 10% as suggested by our

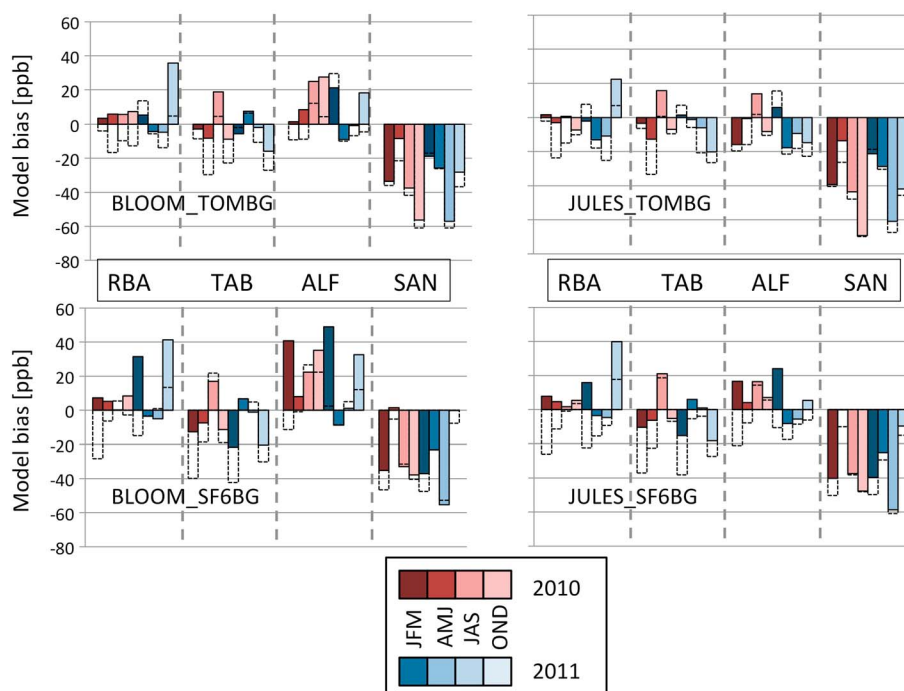


**Figure 9.** Seasonal mean model-observation bias (ppb) prior (dotted bars) and posterior (colored bars) to application of scaling factors at four sites located within the Amazon Basin in 2010 and 2011. Positive numbers indicate model overestimation compared to observations. Left panels use BLOOM wetland model, and right panels use JULES wetland model. Top panels use standard TOMCAT background  $\text{CH}_4$ , and bottom panels use  $\text{SF}_6$ -based background  $\text{CH}_4$ .

prior inventories (although, as mentioned, the GFED inventory does not fully account for smaller fires). After application of  $\lambda^{\text{BB}}$ , the scaling factors applied to the remaining South American emissions produces larger total annual emissions than those of the prior inventories, as a result of the generally negative model biases at RBA and TAB. Depending on the WL/R inventory and the model background  $\text{CH}_4$  values used, we find annual  $\text{CH}_4$  emissions in 2010 of 36.5–41.1 Tg and annual emissions of 31.6–38.8 Tg in 2011. Our prior annual emissions are 32.4–33.5 Tg( $\text{CH}_4$ )/yr in 2010 and 28.8–29.0 Tg( $\text{CH}_4$ )/yr, and so the posterior emissions are larger than the respective prior in both cases. The mean increase compared to the prior is 6.4 Tg/yr in 2010 (significant at the 95% confidence level using a student's  $t$  test) and 6.2 Tg/yr in 2011 (significant at the 90% confidence level). As a result, the annual mean absolute bias (MAB) between the simulated and observed regional contributions is reduced at all sites (including SAN) during both years when using the JULES wetland model and either  $\text{CH}_4$  background estimate (annual MAB reduction ranges from 2% to 68%). Using the scaling method on the BLOOM inventory also generally decreases the annual MAB by up to 65%, except at ALF in 2011 when using the  $\text{SF}_6$ -based background and at RBA in 2011 when using either background. It may be that the geographical distribution of the BLOOM inventory is incompatible with the attempted simultaneous reduction of the errors across all sites. The inflexibility of the geographical distribution of emissions means that time periods when the model biases at RBA and TAB are large and of opposing signs (e.g., October–December 2010) are difficult to resolve through application of a single scaling factor for the region. An inversion method that independently scales emissions in different regions of the basin would have better success in improving the model performance across all stations.

There are few previous studies that explicitly provide basin-wide estimates of  $\text{CH}_4$  emissions with which to compare our emission estimates. We have summarized the results of previous studies, along with their methodologies and the regions over which their results were reported in Table 4 and along with the results of this study for comparison purposes. *Melack et al.* [2004] up-scaled field measurements of  $\text{CH}_4$  emission rates using remote sensing data to find basin-wide wetland emissions of 29 Tg( $\text{CH}_4$ )/yr (based on a basin area of  $5 \times 10^6 \text{ km}^2$ , using data from the 1980s and 1990s). *Miller et al.* [2007] used observations made at SAN and at another site within the basin, Manaus (59.1°E, 2.3°S), to estimate average basin-wide emissions from all

**Table 4.** Details and Results of Previous Studies That Have Evaluated Emissions of CH<sub>4</sub> (in Tg(CH<sub>4</sub>)/yr) From the Amazon Basin and Tropical South America

	Method Type		Region		Area (million km <sup>2</sup> )	Emission Type	Time Period	Total Emissions (Tg CH <sub>4</sub> )
This study	As Above		Amazon Basin	Amazon Basin	5.8	All Sources	2010/11	31–41
Melack et al. [2004]	Field measurements of emissions + remote sensing	Flooded areas of the Basin below 500 m			~0.7 (but represents entire Basin)	Wetlands	Various	29
Miller et al. [2007]	Modeling + observations at two sites	Amazon Basin			5.0	All sources	2001–2006	49
do Carmo et al. [2006]	Observations at four upland forest sites	Amazon Basin			5.0	All sources	2004/05	4–38
Frankenberg et al. [2008]	Inverse modeling	Tropical South America (180°W–30°W, 15°N–15°S)			~55.0	All sources	2004	79
Bergamaschi et al. [2009]	Inverse modeling	Amazon Basin (80°W–45°W, 5°N–15°S)			~8.6	All sources	2004	47.5–53
Bloom et al. [2012] + extension for this study	Remote sensing + process modeling	Amazon Basin (defined as in this study)			5.8	Wetlands	2003–2011	19.5–20.8
Fraser et al. [2013]	Inverse modeling	Tropical South America (TransCom region)			~9.7	All sources	2009–2011	42.3–49.6
Kirschke et al. [2013]	Group of process (bottom-up) models	Tropical South America (TransCom region)			~9.7	Wetlands	2000–2009	39–92 (mean: 58)
Kirschke et al. [2013]	Group of inverse models	Tropical South America (TransCom region)			~9.7	Wetlands	2000–2009	17–48 (mean: 28)

sources of 49 Tg(CH<sub>4</sub>)/year for the period 2001–2006 (again, based on a basin area of 5 × 10<sup>6</sup> km<sup>2</sup>). However, the authors acknowledged the possibility that the sites used in the study were not representative of the entire basin, and our study supports the premise that use of observations made at SAN would lead to overestimation of basin-wide emissions. *do Carmo et al.* [2006] used CH<sub>4</sub> measurements made at upland forest sites in 2004 and 2005 to derive basin-wide emissions of 4–38 Tg(CH<sub>4</sub>)/yr over a basin region of 5 × 10<sup>6</sup> km<sup>2</sup>, although the relative contribution of different sources was not known and observations were relatively sparse. *Frankenberg et al.* [2008] performed an inversion using ground-based observations and remote sensing observations from Scanning Imaging Absorption Spectrometer for Atmospheric Chartography (SCIAMACHY) to find total emissions of 79 Tg(CH<sub>4</sub>)/yr for Tropical South America (defined as the region (180°W–30°W, 15°N–15°S), a region much larger than that examined in this study, approximately 5.5 × 10<sup>7</sup> km<sup>2</sup>) in 2004. *Bergamaschi et al.* [2009] also used SCIAMACHY data to find total Amazonian emissions of 47.5–53 Tg(CH<sub>4</sub>)/yr in 2004 for a region of area 8.6 × 10<sup>6</sup> km<sup>2</sup>, of which 40–42 Tg(CH<sub>4</sub>)/yr were from WL/R sources. More recently, *Fraser et al.* [2013] performed an inversion using in situ and remote sensing observations to find emissions of 42.3–49.6 Tg(CH<sub>4</sub>)/yr from Tropical South America (once more, a larger region than used in this study, ~9.7 × 10<sup>6</sup> km<sup>2</sup>) in 2009 and 2010, while *Kirschke et al.* [2013] estimated wetland emissions from the same Tropical South American region in 2000–2009 to be 17–48 Tg(CH<sub>4</sub>)/yr (mean: 28 Tg(CH<sub>4</sub>)/yr) using a group of inversion results and 39–92 Tg(CH<sub>4</sub>)/yr (mean: 58 Tg(CH<sub>4</sub>)/yr) using a suite of process models. They found that bottom-up models estimated much larger emissions from Tropical South America than those that used top-down methods.

Together, these previous studies provide relatively wide bounds of 4–92 Tg(CH<sub>4</sub>)/yr for basin emissions. However, with the exception of *Melack et al.* [2004] and the top-down models in *Kirschke et al.* [2013], the previous studies generally indicate larger emissions than we report here. Those two

studies do agree fairly well with each other and with our findings, however. In most cases, there are clear responsible factors for the discrepancy between our results and the findings of other studies, such as the reporting of emissions over regions larger than only the Amazon Basin, up-scaling of results of measurements from relatively few locations or, in the case of *Miller et al.* [2007], the reliance on observations made at sites which are now known not to be representative of the entire basin. Assessing the level of agreement between this work and previous studies is therefore difficult, but our estimates fall well within the boundaries of previous work, and significantly reduce the associated uncertainties.

#### 4.4. Response of Amazon CH<sub>4</sub> to Changing Meteorological Conditions

The different governing meteorological conditions in 2010 and 2011 provide an opportunity to examine the sensitivity of CH<sub>4</sub> emissions in the Amazon to changes in temperature and precipitation. Figure 2 shows the precipitation and temperature variations in the basin in 2010 and 2011 compared with the mean over the period 2004–2011. 2010 was significantly drier and warmer than usual across almost the entire basin. February and March were extremely warm and dry (anomalies in these months > 1 $\sigma$  from the average), as were September and October. Rainfall and temperature in May–August returned toward average values for the period. The most significant departures from the average temperature and precipitation values were in early 2010, and during this time the regional component of the observed CH<sub>4</sub> concentration is highly dependent upon whether the standard or SF<sub>6</sub>-based background concentration is used, particularly at the western sites. Assuming that the SF<sub>6</sub>-based background is correct suggests that the high temperatures in the region led to significant regional emissions despite the significantly reduced rainfall, but this cannot be inferred from the standard model background. However, both backgrounds indicate enhancements at RBA, TAB, and ALF during April–May 2010, corresponding with the period when the temperature was still significantly above average and total precipitation increased back toward average. This may imply that the sudden increase in rainfall combined with elevated temperatures led to increased microbial CH<sub>4</sub> emissions during these months. The drought also led to increased BB emissions later in 2010 although, as discussed, observed atmospheric CH<sub>4</sub> concentrations are not affected as greatly by these combustion emissions as they are in the model.

The increased precipitation in 2011 occurred mostly toward the east of the basin between January and April, when temperatures were cooler than average. However, the dry season in 2011 was actually drier and warmer than that of 2010. The last few months of 2011 returned toward average values.

The observed regional concentrations are relatively low at the beginning of 2011, corresponding to the period of low temperatures. However, throughout the remainder of the year, concentrations are similar to those of 2010, with significant enhancements seen at all sites despite only a very small contribution from BB emissions. It is possible that the combination of high rainfall totals early in the year combined with high temperatures in July and August led to ideal conditions for microbial emissions in the basin throughout the middle of 2011.

Our analysis suggests that the meteorological variations between the two years may have had little effect on the magnitude of the noncombustion emissions of CH<sub>4</sub> into the atmosphere from the Amazon Basin. The scaling factor analysis infers noncombustion emissions of 33.4–38.0 Tg/yr in 2010 and 31.0–38.2 Tg/yr in 2011. Due to the relatively small number of observations used to derive these values and the remaining model-observation error after the analysis, the differences between the two ranges is not significant (the difference between emissions in 2010 and 2011 is not significant at the 90% confidence level using a student's *t* test). Assuming that anthropogenic emissions were relatively stable between the two years, this therefore suggests that wetland emissions in the region were fairly consistent in 2010 and 2011, although the range of uncertainty in these estimates does allow for some variation. While it may be counter intuitive that basin-wide wetland emissions could have been similar during 2 years with very different meteorological regimes, it may have been that increased temperatures in early 2010 offset the effect of the reduced precipitation. These results indicate that variations in surface temperature may have had an important effect on basin-wide emissions of WL/R CH<sub>4</sub> emissions in each of these meteorologically atypical years. One possibility is that decreased water table depth during the drought conditions of 2010 actually led to enhanced methane emission rates due to increased ebullition rates in drought-afflicted inundated regions as a result of lower levels of hydrostatic pressure for gas bubbles to overcome. In addition, the increased tree mortality due to the drought conditions [Lewis et al., 2011] may be another underlying cause for increased CH<sub>4</sub> emissions

during that year. This increase in mortality may have led to a temporary increase in the available carbon substrate in inundated areas.

However, other possible reasons for our findings include (i) oversensitivity to the western side of the basin, where the precipitation differences were less pronounced between 2010 and 2011 than toward the eastern side (see Figure 2), due to our decision to exclude SAN from the analysis and the small weighting given to ALF; (ii) the relatively small number of total observations used in finding  $\lambda$ ; (iii) the inflexibility of the geographical distribution of basin-wide emissions when finding  $\lambda$ ; and (iv) inherent difficulties in simulating the background methane concentrations in the basin even after the use of SF<sub>6</sub> observations to constrain it. Indeed, our findings are in contrast of those of Bloom *et al.* [2010], who found that water table depth was the strongest factor for determining wetland CH<sub>4</sub> emissions in tropical regions and that 2010 had much smaller WL/R emissions than 2011. Further investigation into the role of temperature and precipitation variations on Amazon wetland emissions during 2010 and 2011 is necessary to support our finding. Further understanding of the processes governing methane emission into the atmosphere would also help to improve bottom-up models, which are currently not in good agreement, especially in the Amazon region [e.g., Melton *et al.*, 2013].

## 5. Summary

We have used the TOMCAT CTM to analyze a new set of in situ observations from 2010 and 2011 that are representative of the majority of the Amazon Basin in order to provide a constraint for basin CH<sub>4</sub> emissions and attribute them to source processes. While 2010 was a dry and warm year, 2011 was much wetter and somewhat cooler, allowing some assessment of the sensitivity of CH<sub>4</sub> emissions to climate variations. We find that the observations do not display a significant seasonal cycle, although this is partly due to variations in transport of background CH<sub>4</sub> masking changes in South American emissions. Background CH<sub>4</sub> concentrations are elevated by recent South American emissions by up to 130 ppb, except at SAN where South American emissions contribute as much as 150 ppb to the total atmospheric concentration. Variations in precipitation and temperature between the two years induce changes in the annual mean observed CH<sub>4</sub> of up to 5.5 ppb and alter the timings of enhancements of regional emissions. However, the observed atmospheric concentration at three of the measurement locations increases by less than the observed global growth rate, possibly due to emission changes in the region masking changes to the background CH<sub>4</sub> concentration.

We used estimates of wetland emissions from two models, one a top-down model and one a process-based bottom-up model. While the geographical distribution produced by the two models is different, the total basin-wide emissions are within 1 Tg of each other in both years. This leads to similar performances when the atmospheric model is compared to the observations regardless of which model is used.

Estimating the background CH<sub>4</sub> concentration at each of the sites allows us to assess the contribution of regional sources only to the observed concentration but relies on accurate model performance. In order to attempt to improve the accuracy of the simulated background concentrations, we applied a correction to the model background based on observed SF<sub>6</sub> concentrations. This significantly reduced the magnitude of the seasonal cycle of background CH<sub>4</sub> at each site and therefore led to larger estimates of basin-wide emissions, by up to 4.2 Tg in 2010 and up to 7.2 Tg in 2011.

When using the standard model background CH<sub>4</sub> concentrations, there is generally good agreement ( $r^2 > 0.2$ ,  $p < 0.01$ , MB < 9.5 ppb) between the simulated and observed CH<sub>4</sub> at TAB, RBA, and ALF. In contrast, the model is not able to capture the magnitude or seasonality of variations at SAN, the site located in the northeast of the basin. This might indicate significant emissions near SAN that are not included in the model, although, due to the methodology of this study, this relies on the accuracy of the simulated background concentrations. Use of the SF<sub>6</sub>-based background concentrations, however, reduces the accuracy of the model performance in comparison with the observations.

Our prior combined wetland and rice emissions from the wetland models were 19.5–20.6 Tg(CH<sub>4</sub>)/yr in 2010 and 20.8–21.0 Tg(CH<sub>4</sub>)/yr in 2011, the relatively small variation indicating robustness against changes in local precipitation and temperature. Since rice cultivation is not significant within the basin, this total is made up almost exclusively of wetland emissions. Based on simple statistical analysis using observed and simulated CH<sub>4</sub> at TAB, RBA, and ALF, we find posterior basin-wide noncombustion emissions of CH<sub>4</sub> of

33.4–38.0 Tg/yr in 2010 and 31.0–38.2 Tg/yr in 2011, significantly reducing the uncertainty surrounding previous estimates due to the new observations of CH<sub>4</sub> concentrations within the basin. However, the uncertainty still associated with these estimates is greater than the interannual variability displayed by the prior emission estimates, meaning that it is not possible to ascertain whether the different prevailing conditions over the basin in 2010 and 2011 significantly affected the total wetland emissions from the region.

Comparison of the modeled and observed CH<sub>4</sub> and CO indicates that biomass burning emissions in 2010 were approximately a factor of 6 larger than those in 2011, not a factor of 11 as assumed in the prior emissions taken from the GFED v3.1 inventory. This is mainly due to a reduction of 42% in 2010 compared to the prior emissions, when drought conditions led to significant levels of biomass burning compared to this during the following wetter year. The relatively good model simulation of CO at SAN indicates that the large observed enhancements of the CH<sub>4</sub> concentration at the same site, which are not captured in the model simulations, were likely to be microbial in nature, rather than originating from combustion sources.

The forward model study described here is a good precursor to a potential inverse modeling study, in which a model could be used to optimize the emissions of CH<sub>4</sub> so that model-observation differences are minimized, such as in *Bergamaschi et al.* [2009] and *Fraser et al.* [2013]. In such a study, the new observation data set described here may be assimilated within the inversion or held back in order to provide validation of results. We plan to use the inverse model described in *Wilson et al.* [2014] in order to perform a top-down analysis of Amazon CH<sub>4</sub> emissions. Current satellite platforms including Greenhouse gases Observing SATellite [Kuze et al., 2009; Parker et al., 2011] and Infrared Atmospheric Sounding Interferometer [Razavi et al., 2009] are both able to provide remote sensing observations of methane that cover the Amazon Basin. Inverse modeling methods have the advantage that they provide information regarding the spatial distribution of emissions from within the basin, and might highlight regions with significant emissions not manifesting in bottom-up models, such as at SAN, where it would be beneficial to further investigate the mechanisms governing natural CH<sub>4</sub> emission rates.

#### Acknowledgments

CH<sub>4</sub>, CO, and SF<sub>6</sub> vertical profile observations made as part of the AMAZONICA project will be made available through the World Meteorological Organisation's repository, the World Data Center for Greenhouse Gases (<http://ds.data.jma.go.jp/gmd/wdcgg/>) soon after publication of this manuscript. This work was supported by the UK Natural Environment Research Council (NERC) and the National Centre for Earth Observation (NCEO). Financial support was from the NERC Consortium grants for AMAZONICA (NE/F005806/1) and the Amazon hydrological cycle (NE/K01353X/1), along with the EU 7th Framework GEOCARBON project grant (grant agreement 283080), CNPq and FAPESP. M.G. also acknowledges a bolsa from the Brazilian ciencia sem fronteiras program and a visiting fellowship at CIRES and NOAA/ESRL and LG support from CNPq, CAPES, and FAPESP. J.B.M. thanks the NOAA Climate Program Office's Atmospheric Chemistry, Carbon Cycle, and Climate (AC4) program for support, including that for collection and analysis of NOAA CH<sub>4</sub> observations used in this study. MPC is partly funded by a Royal Society Wolfson Merit Award. The TOMCAT simulations were run on the UK National Supercomputing Service ARCHER and University of Leeds ARC2 computing facilities. We thank Wuhu Feng (NCAS) for help with the TOMCAT model and Andrew Croftwell (NOAA) for instrument development.

Our study provides for the first time an estimate of Amazon CH<sub>4</sub> emissions based on in situ measured data representative of the entire basin [Gatti et al., 2014], which provides higher sensitivity to local surface emissions than possible when using remote sensing methods and also avoids the potential biases of such approaches. The posterior basin-wide CH<sub>4</sub> emissions reduce the annual mean absolute bias at each individual measurement site, except in some cases when using the BLOOM emissions. Our analysis suggests that Amazonian emissions contributed between 5.5% and 7.5% of global CH<sub>4</sub> emissions during this time (assuming global emissions of 556 Tg CH<sub>4</sub>/yr [Ciais et al., 2013], despite small contributions from anthropogenic sources within the basin. This is a significant contribution to the global atmospheric CH<sub>4</sub> budget and given that anthropogenic emissions of CH<sub>4</sub> contribute up to 65% of the total methane flux into the atmosphere [Prather et al., 2012], this means that the basin may emit 14–20% of the planet's natural emissions of CH<sub>4</sub>. This is a highly significant contribution from a region that covers approximately 4% of the planet's land surface area (assuming global land surface area of  $1.47 \times 10^8$  km<sup>2</sup> and Amazon Basin area of  $6 \times 10^6$  km<sup>2</sup>).

#### References

- Aragão, L. E. O. C., Y. Malhi, N. Barbier, A. Lima, Y. Shimabukuro, L. Anderson, and S. Saatchi (2008), Interactions between rainfall, deforestation and fires during recent years in the Brazilian Amazonia, *Phil. Trans. R. Soc. B*, *363*, 1779–1785.
- Aydin, M., K. R. Verhulst, E. S. Saltzman, M. O. Battle, S. A. Montzka, D. R. Blake, Q. Tang, and M. J. Prather (2011), Recent decreases in fossil-fuel emissions of ethane and methane derived from firn air, *Nature*, *476*, 198–201.
- Beck, C., J. Grieser, and B. Rudolf (2005), A new monthly precipitation climatology for the global land areas for the period 1951 to 2000, *Geophys. Res. Abstr.*, *7*, 07154.
- Bergamaschi, P., et al. (2009), Inverse modeling of global and regional CH<sub>4</sub> emissions using SCIAMACHY satellite retrievals, *J. Geophys. Res.*, *114*, D22301, doi:10.1029/2009JD012287.
- Bloom, A. A., P. I. Palmer, A. Fraser, D. S. Reay, and C. Frankenberg (2010), Large-scale controls of methanogenesis inferred from methane and gravity spaceborne data, *Science*, *327*, 322–325.
- Bloom, A. A., P. I. Palmer, A. Fraser, and D. S. Reay (2012), Seasonal variability of tropical wetland CH<sub>4</sub> emissions: The role of the methanogen-available carbon pool, *Biogeosciences*, *9*, 2821–2830.
- Bloom, A. A., J. Worden, Z. Jiang, H. Worden, T. Kurosu, C. Frankenberg, and D. Schimel (2015), Remote-sensing constraints on South America fire traits by Bayesian fusion of atmospheric and surface data, *Geophys. Res. Lett.*, *42*, 1268–1274, doi:10.1002/2014GL062584.
- Bousquet, P., et al. (2006), Contribution of anthropogenic and natural sources to atmospheric methane variability, *Nature*, *443*, 439–443.
- Cao, M., S. Marshall, and K. Gregson (1996), Global carbon exchange and methane emissions from natural wetlands: Application of a process-based model, *J. Geophys. Res.*, *101*, 14,399–14,414, doi:10.1029/96JD00219.

- Chipperfield, M. P. (2006), New version of the TOMCAT/SLIMCAT off-line chemical transport model: Intercomparison of stratospheric tracer experiments, *Q. J. R. Meteorol. Soc.*, *132*, 1179–1203.
- Chipperfield, M. P., D. Cariolle, P. Simon, R. Ramarosan, and D. J. Lary (1993), A three-dimensional modeling study of trace species in the Arctic lower stratosphere during winter 1989–1990, *J. Geophys. Res.*, *98*, 7199–7218, doi:10.1029/92JD02977.
- Ciais, P., et al. (2013), Carbon and other biogeochemical cycles, in *Climate Change 2013: The Physical Science Basis. Contribution of Working Group I to the Fifth Assessment Report of the Intergovernmental Panel on Climate Change*, edited by T. F. Stocker et al., Cambridge Univ. Press, Cambridge, U. K., and New York.
- Clark, D. B., et al. (2011), The Joint UK Land Environment Simulator (JULES), model description—Part 2: Carbon fluxes and vegetation dynamics, *Geosci. Model Dev.*, *4*, 701–722.
- Dee, D. P., et al. (2011), The ERA-Interim reanalysis: Configuration and performance of the data assimilation system, *Q. J. R. Meteorol. Soc.*, *137*, 553–597.
- Dlugokencky, E. J., E. G. Nisbet, R. Fisher, and D. Lowry (2011), Global atmospheric methane: Budget, changes and dangers, *Philos. Trans. R. Soc. A*, *369*, 2058–2072.
- do Carmo, J. B., M. Keller, J. D. Dias, P. B. Camargo, and P. Crill (2006), A source of methane from upland forests in the Brazilian Amazon, *Geophys. Res. Lett.*, *33*, L04809, doi:10.1029/2005GL025436.
- Duncan, B. N., J. A. Logan, I. Bey, I. A. Megretskaia, R. M. Yantosca, P. C. Novelli, N. B. Jones, and C. P. Rinsland (2007), Global budget of CO<sub>2</sub> 1988–1997: Source estimates and validation with a global model, *J. Geophys. Res.*, *112*, D22301, doi:10.1029/2007JD008459.
- Etiopie, G., and A. V. Milkov (2004), A new estimate of global methane flux from onshore and shallow submarine mud volcanoes to the atmosphere, *Environ. Geol.*, *46*, 997–1002.
- Fan, Y., and H. van den Dool (2008), A global monthly land surface air temperature analysis for 1948–present, *J. Geophys. Res.*, *113*, D01103, doi:10.1029/2007JD008470.
- Fiore, A. M., J. J. West, L. W. Horowitz, V. Naik, and M. D. Schwarzkopf (2008), Characterizing the tropospheric ozone response to methane emission controls and the benefits to climate and air quality, *J. Geophys. Res.*, *113*, D08307, doi:10.1029/2007JD009162.
- Frankenberg, C., J. F. Meirink, P. Bergamaschi, A. P. H. Goede, M. Heimann, S. Körner, U. Platt, M. van Weele, and T. Wagner (2006), Satellite cartography of atmospheric methane from SCIAMACHY on board ENVISAT: Analysis of the years 2003 and 2004, *J. Geophys. Res.*, *111*, D07303, doi:10.1029/2005JD006235.
- Frankenberg, C., P. Bergamaschi, A. Butz, S. Houweling, J. F. Meirink, J. Notholt, A. K. Petersen, H. Schrijver, T. Warneke, and I. Aben (2008), Tropical methane emissions: A revised view from SCIAMACHY onboard ENVISAT, *Geophys. Res. Lett.*, *35*, L15811, doi:10.1029/2008GL034300.
- Fraser, A., et al. (2013), Estimating regional methane surface fluxes: The relative importance of surface and GOSAT mole fraction measurements, *Atmos. Chem. Phys.*, *13*, 5697–5713.
- Fung, I., J. John, J. Lerner, E. Matthews, M. Prather, L. P. Steele, and P. J. Fraser (1991), Three-dimensional model synthesis of the global methane cycle, *J. Geophys. Res.*, *96*, 13,033–13,065, doi:10.1029/91JD01247.
- Gatti, L. V., et al. (2014), Drought sensitivity of Amazonian carbon balance revealed by atmospheric measurements, *Nature*, *506*, 76–80.
- Gedney, N., P. M. Cox, and C. Huntingford (2004), Climate feedback from wetland emissions, *Geophys. Res. Lett.*, *31*, L20503, doi:10.1029/2004GL020919.
- Granier, C., J. Lamarque, A. Mieville, J. Muller, J. Olivier, J. Orlando, J. Peters, G. Petron, G. Tyndall, and S. Wallens (2005), POET. [Available at <http://www.aero.jussieu.fr/projet/ACCENT/POET.php>]
- Guenther, A., T. Karl, P. Harley, C. Wiedinmyer, P. I. Palmer, and C. Geron (2006), Estimates of global terrestrial isoprene emissions using MEGAN (Model of Emissions of Gases and Aerosols from Nature), *Atmos. Chem. Phys.*, *6*, 3181–3210.
- Gurney, K. R., et al. (2002), Towards robust regional estimates of CO<sub>2</sub> sources and sinks using atmospheric transport models, *Nature*, *415*, 626–630.
- Hossaini, R., et al. (2013), Evaluating global emission inventories of biogenic bromocarbons, *Atmos. Chem. Phys.*, *13*, 11,819–11,838.
- Houweling, S., T. Kaminski, F. Dentener, J. Lelieveld, and M. Heimann (1999), Inverse modeling of methane sources and sinks using the adjoint of a global transport model, *J. Geophys. Res.*, *104*, 26,137–26,160, doi:10.1029/1999JD900428.
- Huijnen, V., et al. (2010), The global chemistry transport model TM5: Description and evaluation of the tropospheric chemistry version 3.0, *Geosci. Model Dev.*, *3*, 445–473.
- Kai, F. M., S. C. Tyler, J. T. Randerson, and D. R. Blake (2011), Reduced methane growth rate explained by decreased Northern Hemisphere microbial sources, *Nature*, *476*, 194–197.
- Kaiser, J. W., et al. (2012), Biomass burning emissions estimated with a global fire assimilation system based on observed fire radiative power, *Biogeosciences*, *9*, 527–554.
- Kirschke, S., et al. (2013), Three decades of global methane sources and sinks, *Nat. Geosci.*, *6*, 813–823.
- Kuze, A., H. Suto, M. Nakajima, and T. Hamazaki (2009), Thermal and near infrared sensor for carbon observation Fourier-transform spectrometer on the Greenhouse Gases Observing Satellite for greenhouse gases monitoring, *Appl. Opt.*, *48*, 6716–6733.
- Lamarque, J.-F., et al. (2010), Historical (1850–2000) gridded anthropogenic and biomass burning emissions of reactive gases and aerosols: Methodology and application, *Atmos. Chem. Phys.*, *10*, 7017–7039.
- Lambert, G., and S. Schmidt (1993), Reevaluation of the oceanic flux of methane: Uncertainties and long term variations, *Chemosphere*, *26*, 579–589.
- Landerer, F. W., and S. C. Swenson (2012), Accuracy of scaled GRACE terrestrial water storage estimates, *Water Resour. Res.*, *48*, W04531, doi:10.1029/2011WR011453.
- Levin, I., et al. (2010), The global SF<sub>6</sub> source inferred from long-term high precision atmospheric measurements and its comparison with emission inventories, *Atmos. Chem. Phys.*, *10*, 2655–2662.
- Levin, I., C. Veidt, B. H. Vaughn, G. Brailsford, T. Bromley, R. Heinz, D. Lowe, J. B. Miller, C. Poß, and J. W. C. White (2012), No inter-hemispheric  $\delta^{13}\text{C}_{\text{CH}_4}$  trend observed, *Nature*, *486*, E3–E4.
- Lewis, S. L., P. M. Brandt, O. L. Phillips, G. M. F. van der Heijden, and D. Nepstad (2011), The 2010 Amazon drought, *Science*, *331*, 554–554.
- Li, W., R. Fu, and R. E. Dickinson (2006), Rainfall and its seasonality over the Amazon in the 21st century as assessed by the coupled models for the IPCC AR4, *J. Geophys. Res.*, *111*, D02111, doi:10.1029/2005JD006355.
- Malhi, Y., J. T. Roberts, R. A. Betts, T. J. Killeen, W. Li, and C. A. Nobre (2008), Climate Change, Deforestation, and the Fate of the Amazon, *Science*, *319*, 169–172.
- Marengo, J. A., J. Tomasella, L. M. Alves, W. R. Soares, and D. A. Rodriguez (2011), The drought of 2010 in the context of historical droughts in the Amazon region, *Geophys. Res. Lett.*, *38*, L12703, doi:10.1029/2011GL047436.

- Marthews, T. R., S. J. Dadson, B. Lehner, S. Abele, and N. Gedney (2015), High-resolution global topographic index values for use in large-scale hydrological modelling, *Hydrol. Earth Syst. Sci.*, *19*, 91–104.
- Matthews, E., and I. Fung (1987), Methane emission from natural wetlands: Global distribution, area, and environmental characteristics of sources, *Global Biogeochem. Cycles*, *1*, 61–86, doi:10.1029/GB001i001p00061.
- McNorton, J., et al. (2016), Role of OH variability in the stalling of the global atmospheric CH<sub>4</sub> growth rate from 1999 to 2006, *Atmos. Chem. Phys. Discuss.*, doi:10.5194/acp-2015-1029, in press.
- Melack, J. M., L. L. Hess, M. Gastil, B. R. Forsberg, S. K. Hamilton, I. B. T. Lima, and E. M. L. M. Novo (2004), Regionalization of methane emissions in the Amazon Basin with microwave remote sensing, *Global Change Biol.*, *10*, 530–544.
- Melton, J. R., et al. (2013), Present state of global wetland extent and wetland methane modelling: Conclusions from a model inter-comparison project (WETCHIMP), *Biogeosciences*, *10*, 753–788.
- Miller, J. B., L. V. Gatti, M. T. S. d'Amelio, A. M. Croftwell, E. J. Dlugokencky, P. Bakwin, P. Artaxo, and P. P. Tans (2007), Airborne measurements indicate large methane emissions from the eastern Amazon Basin, *Geophys. Res. Lett.*, *34*, L10809, doi:10.1029/2006GL029213.
- Monks, S. A., S. R. Arnold, and M. P. Chipperfield (2012), Evidence for El Niño–Southern Oscillation (ENSO) influence on Arctic CO interannual variability through biomass burning emissions, *Geophys. Res. Lett.*, *39*, L14804, doi:10.1029/2012GL052512.
- Monks, S. A., et al. (2015), Multi-model study of chemical and physical controls on transport of anthropogenic and biomass burning pollution to the Arctic, *Atmos. Chem. Phys.*, *15*, 3575–3603.
- Montzka, S. A., M. Krol, E. Dlugokencky, B. Hall, P. Jöckel, and J. Lelieveld (2011), Small interannual variability of global atmospheric hydroxyl, *Science*, *331*, 67–69.
- Myhre, G., et al. (2013), Anthropogenic and natural radiative forcing, in *Climate Change 2013: The Physical Science Basis. Contribution of Working Group I to the Fifth Assessment Report of the Intergovernmental Panel on Climate Change*, edited by T. F. Stocker et al., Cambridge Univ. Press, Cambridge, U. K., and New York.
- Nisbet, E. G., E. J. Dlugokencky, and P. Bousquet (2014), Methane on the rise—Again, *Science*, *343*, 493–495.
- Olivier, J., and J. Berdowski (2001), Global emission sources and sinks, in *The Climate System*, edited by J. Berdowski, R. Guicherit, and B. Heij, pp. 33–78, A. A. Balkema Publishers Swets Zeitlinger Publishers, Lisse, Netherlands.
- Olivier, J., J. Peters, C. Granier, G. Petron, J. Müller, and S. Wallens (2003), Present and future surface emissions of atmospheric compounds, *POET Rep. 2, EU Proj. EVK2-1999*, 11.
- Parker, R., et al. (2011), Methane observations from the Greenhouse Gases Observing SATellite: Comparison to ground-based TCCON data and model calculations, *Geophys. Res. Lett.*, *38*, L15807, doi:10.1029/2011GL047871.
- Patra, P. K., et al. (2009), Growth rate, seasonal, synoptic, diurnal variations and budget of methane in the lower atmosphere, *J. Meteorol. Soc. Jpn. Ser. II*, *87*, 635–663.
- Patra, P. K., et al. (2011), TransCom model simulations of CH<sub>4</sub> and related species: Linking transport, surface flux and chemical loss with CH<sub>4</sub> variability in the troposphere and lower stratosphere, *Atmos. Chem. Phys.*, *11*, 12,813–12,837.
- Pison, I., B. Ringeval, P. Bousquet, C. Prigent, and F. Papa (2013), Stable atmospheric methane in the 2000s: Key-role of emissions from natural wetlands, *Atmos. Chem. Phys.*, *13*, 11,609–11,623.
- Poulter, B., L. Aragão, U. Heyder, M. Gumpenberger, J. Heinke, F. Langerwisch, A. Rammig, K. Thonicke, and W. Cramer (2010), Net biome production of the Amazon Basin in the 21st century, *Global Change Biol.*, *16*, 2062–2075.
- Prather, M., et al. (2001), Atmospheric chemistry and greenhouse gases, in *Climate Change 2001, The Scientific Basis: Contribution of Working Group I to the Third Assessment Report of the Intergovernmental Panel on Climate*, edited by J. T. Houghton et al., 881 pp., Cambridge Univ. Press, Cambridge, U. K., and New York.
- Prather, M. J., C. D. Holmes, and J. Hsu (2012), Reactive greenhouse gas scenarios: Systematic exploration of uncertainties and the role of atmospheric chemistry, *Geophys. Res. Lett.*, *39*, L09803, doi:10.1029/2012GL051440.
- Prinn, R. G., et al. (2005), Evidence for variability of atmospheric hydroxyl radicals over the past quarter century, *Geophys. Res. Lett.*, *32*, L07809, doi:10.1029/2004GL022228.
- Razavi, A., C. Clerbaux, C. Wespes, L. Clarisse, D. Hurtmans, S. Payan, C. Camy-Peyret, and P. F. Coheur (2009), Characterization of methane retrievals from the IASI space-borne sounder, *Atmos. Chem. Phys.*, *9*, 7889–7899.
- Richards, N. A. D., S. R. Arnold, M. P. Chipperfield, G. Miles, A. Rap, R. Siddans, S. A. Monks, and M. J. Hollaway (2013), The Mediterranean summertime ozone maximum: Global emission sensitivities and radiative impacts, *Atmos. Chem. Phys.*, *13*, 2331–2345.
- Rigby, M., et al. (2008), Renewed growth of atmospheric methane, *Geophys. Res. Lett.*, *35*, L22805, doi:10.1029/2008GL036037.
- Ringeval, B., N. de Noblet-Ducoudré, P. Ciais, P. Bousquet, C. Prigent, F. Papa, and W. B. Rossow (2010), An attempt to quantify the impact of changes in wetland extent on methane emissions on the seasonal and interannual time scales, *Global Biogeochem. Cycles*, *24*, GB2003, doi:10.1029/2008GB003354.
- Sander, S. P., et al. (2006), Chemical kinetics and photochemical data for use in atmospheric studies, Evaluation Number 15, JPL Publication 06-2, Jet Propul. Lab., Calif. Inst. of Technol., Pasadena, Calif.
- Simpson, I. J., M. P. Sulbaek Andersen, S. Meinardi, L. Bruhwiler, N. J. Blake, D. Helmig, F. S. Rowland, and D. R. Blake (2012), Long-term decline of global atmospheric ethane concentrations and implications for methane, *Nature*, *488*, 490–494.
- Spivakovsky, C. M., et al. (2000), Three-dimensional climatological distribution of tropospheric OH: Update and evaluation, *J. Geophys. Res.*, *105*, 8931–8980, doi:10.1029/1999JD901006.
- Stockwell, D. Z., and M. P. Chipperfield (1999), A tropospheric chemical-transport model: Development and validation of the model transport schemes, *Q. J. R. Meteorol. Soc.*, *125*, 1747–1783.
- van der Werf, G. R., J. T. Randerson, L. Giglio, G. J. Collatz, M. Mu, P. S. Kasibhatla, D. C. Morton, R. S. DeFries, Y. Jin, and T. T. van Leeuwen (2010), Global fire emissions and the contribution of deforestation, savanna, forest, agricultural, and peat fires (1997–2009), *Atmos. Chem. Phys.*, *10*, 11,707–11,735.
- Velders, G. (1995), Description of the RIVM 2-dimensional stratosphere model, *RIVM Rep. 722201002*, Netherlands.
- Wilson, C., M. P. Chipperfield, M. Gloor, and F. Chevallier (2014), Development of a variational flux inversion system (INVICAT v1.0) using the TOMCAT chemical transport model, *Geosci. Model Dev.*, *7*, 2485–2500.
- Yan, X., H. Akiyama, K. Yagi, and H. Akimoto (2009), Global estimations of the inventory and mitigation potential of methane emissions from rice cultivation conducted using the 2006 Intergovernmental Panel on Climate Change Guidelines, *Global Biogeochem. Cycles*, *23*, GB2002, doi:10.1029/2008GB003299.
- Zeng, N., J.-H. Yoon, J. A. Marengo, A. Subramaniam, C. A. Nobre, A. Mariotti, and J. D. Neelin (2008), Causes and impacts of the 2005 Amazon drought, *Environ. Res. Lett.*, *3*, 014002.